An AI-guided invariant signature places MIS-C with Kawasaki disease in a continuum of host immune responses

Authors: Debashis Sahoo[1,2,3] * ¶, Gajanan D. Katkar[4¶], Chisato Shimizu[2,5], ¶, Jihoon Kim[6], Soni Khandelwal[1], Adriana H. Tremoulet[2,5], John Kanegaye[5], Joseph Bocchini[7], Soumita Das[8], and Jane C. Burns[2,5]*, Pradipta Ghosh[3,4,9,10]*, Pediatric Emergency Medicine Kawasaki Disease Research Group

Collaborators
Pediatric Emergency Medicine Kawasaki Disease Research Group: Naomi Abe, Amy Bryl, J. Joelle Donofrio-Ödmann, Atim Ekpenyong, Michael Gardiner, David J. Gutglass, Jim R. Harley, Margaret B. Nguyen, Kristy Schwartz, Stacey Ulrich,

Affiliations:
[1]Department of Computer Science and Engineering, Jacob's School of Engineering, University of California San Diego.
[2]Department of Pediatrics, University of California San Diego.
[3]Rebecca and John Moore Comprehensive Cancer Center, University of California San Diego.
[4]Department of Cellular and Molecular Medicine, University of California San Diego.
[5]Rady Children's Hospital-San Diego, San Diego, CA
[6]Department of Biomedical informatics, University of California San Diego.
[7]Willis-Knighton Health System, Shreveport, LA
[8]Department of Pathology, University of California San Diego.
[9]Department of Medicine, University of California San Diego.
[10]Veterans Affairs Medical Center, La Jolla, CA.

Conflict of interest statement: Authors have declared that no conflict of interest exists.

¶ Equal contribution.

***Correspondence to**:

Debashis Sahoo, Ph.D; Assistant Professor, Department of Pediatrics, University of California San Diego; 9500 Gilman Drive, MC 0703, Leichtag Building 132; La Jolla, CA 92093-0831.
Phone: 858-246-1803: Fax: 858-246-0019: Email: dsahoo@ucsd.edu

Jane C. Burns, M.D.; Director, Kawasaki Disease Research Center, Department of Pediatrics, University of California San Diego; 9500 Gilman Dr. MC 0641, La Jolla, CA 92093-0641
Phone: 858-246-0155: Email: jcburns@health.ucsd.edu

Pradipta Ghosh, M.D.; Professor, Departments of Medicine, and Cell and Molecular Medicine, University of California San Diego; 9500 Gilman Drive (MC 0651), George E. Palade Bldg, Rm 232, 239; La Jolla, CA 92093. Phone: 858-822-7633: Fax: 858-822-7636: Email: prghosh@ucsd.edu

Abstract: (184 words)

A significant surge in cases of multisystem inflammatory syndrome in children (MIS-C, also called Pediatric Inflammatory Multisystem Syndrome - PIMS) has been observed amidst the COVID-19 pandemic. MIS-C shares many clinical features with Kawasaki disease (KD), although clinical course and outcomes are divergent. We analyzed whole blood RNA sequences, serum cytokines, and formalin fixed heart tissues from these patients using a computational toolbox of two gene signatures, i.e., the 166-gene viral pandemic (ViP) signature, and its 20-gene severe (s)ViP subset that were developed in the context of SARS-CoV-2 infection and a 13-transcript signature previously demonstrated to be diagnostic for KD. Our analyses revealed that KD and MIS-C are on the same continuum of the host immune response as COVID-19 but diverge with two different cardiac phenotypes. The ViP signatures helped unravel the nature of the host immune response (IL15-centric) in MIS-C and KD, reveal unique targetable cytokine pathways in MIS-C, place MIS-C farther along in the spectrum in severity compared to KD and pinpoint key clinical (reduced cardiac function) and laboratory (thrombocytopenia and eosinopenia) parameters that can be useful to monitor severity.

Key Words:
Artificial Intelligence/Machine Learning
Boolean Equivalent Clusters
Angiotensin Converting Enzyme (ACE)-2
Coronavirus COVID-19
MIS-C (multisystem inflammatory syndrome in children)
Kawasaki Disease
Interleukin 15 (IL15)

INTRODUCTION

Multisystem inflammatory syndrome in children [1] (MIS-C; initially named Pediatric Inflammatory Multisystem Syndrome Temporally associated with SARS-CoV-2, PIMS-TS)[2] is a rare but severe condition that occurs in children and adolescents ~4–6 weeks after exposure to SARS-CoV-2. First reported in April 2020 in a cluster of children in the United Kingdom[3], followed by other regions of the world [4], the syndrome is characterized by fever, and variously accompanied by rash, conjunctival injection, gastrointestinal symptoms, shock, and elevated markers of inflammation and antibodies to SARS-CoV-2 in the majority of patients. Myocardial dysfunction and coronary arterial dilation may resemble those seen in another uncommon childhood condition, Kawasaki Disease (KD). KD is an acute inflammatory disorder predominantly seen in young children. Since it was first described in Japan[5] in 1967, KD has emerged as the most common cause of pediatric acquired heart disease in the developed world[6]. Little is known about the definitive triggers of KD; what is most widely accepted is that KD is largely an immune response to a plethora of infectious or environmental stimuli including viruses, fungi (e.g., *Candida* sp.), and bacteria [7-9]. The host genetic background appears to shape this idiosyncratic inflammatory response to an environmental antigen exposure[9].

On May 14, 2020, the CDC published an online Health Advisory that christened this condition as Multisystem Inflammatory Syndrome in Children (MIS-C) and outlined a case definition[10]. Since then, as the COVID-19 pandemic spread across many countries, cases of MIS-C soared, with features of shock and cardiac involvement requiring ionotropic support [in the critical care setting]. But distinguishing MIS-C from KD, KD shock syndrome[11], and other severe infectious or inflammatory conditions remains a challenge. The need for early diagnostic and prognostic markers of disease severity remains unmet; such markers could objectively guide decisions regarding the appropriateness of the level of care and the timing of initiation of life-saving supportive and therapeutic measures.

We recently showed that a 166-gene signature is conserved in all *vi*ral *p*andemics (ViP), including COVID-19, and a subset of 20-genes within that signature that classifies disease severity[12]. These properties inspired the nomenclatures *ViP* and *severe-ViP* (sViP) signatures, respectively. Here we used the ViP signatures as a starting computational framework to navigate the uncharted territory that is MIS-C and to interrogate the shared and unique features in MIS-C and KD.

RESULTS AND DISCUSSION

A gene signature seen in viral pandemics like COVID-19 is also induced in KD.

We sought to define the host immune response in KD and compare that to COVID-19 using an artificial intelligence (AI)-based approach. To this end, we took advantage of a recently identified analysis of the host immune response in COVID-19 in which over 45,000 transcriptomic datasets of viral pandemics were analyzed to extract a 166-gene signature[12] (**Figure 1A**). Because publicly available transcriptomic datasets from SARS-CoV-2-infected patients are still relatively few, the rigor of analysis was increased through the use of an informatics approach, i.e., Boolean Equivalent Correlated Clusters (BECC[13]; **Figure 1A**) that can identify fundamental invariant (universal) gene expression relationships underlying any biological domain; in this case, the biological domain of '*respiratory viral pandemics*' was selected. The 166-gene signature was conserved in all viral pandemics and outbreaks, reflected host immune response to multiple infectious triggers (**Figure 1B**), defined the invariant nature of the host immune response as predominantly IL15/IL15RA-centric, and enabled the formulation of precise therapeutic goals and measurement of therapeutic efficacy[12]. At a molecular level, the *ViP* signatures were distinct from interferon-stimulated genes (ISGs[49,50]), in that, they revealed the broader nature of the host immune response, which included some tell-tale expected (Type I Interferon and cytokine signaling) and some unique (cellular senescence, exhaustion, chromatin silencing, regulation of apoptosis) pathway enrichments[12]. Consequently, the ViP signatures, but not ISGs, were prognostic of disease severity in cohorts of COVID-19 datasets[12].

We used these ViP signatures as quantitative and qualitative framework for measuring the immune response in publicly available historic cohorts of KD predating COVID-19. Both ViP and sViP signatures were upregulated in blood and tissue samples derived from patients with KD compared to healthy controls (ROC AUC for classification of KD vs healthy ranged from 0.8-1.00 across 7 independent cohorts; **Figure 1C**, *left*), and that such induction was limited to the acute phase of KD and downregulated during convalescence (ROC AUC for classification of KD vs healthy ranged from 0.6-0.8 for ViP and 0.8-1.00 for sViP across 4 independent cohorts; **Figure 1C**, middle).

The strength of association between ViP/sViP signatures and acute KD was also preserved in datasets comprised of KD samples prospectively collected before and after IVIG treatment, and treatment response was annotated as responder (R) or non-responder (NR) (**Figure 1C**, right). First, sex had no impact on the induction of signatures (ROC AUC 0.6 in Males vs Females). Second, although the ViP/sViP signatures did not predict treatment response to IVIG (ROC AUC 0.5-0.6 in pre-treatment samples R vs NR; GSE63881 and GSE9864), they were reduced in all responders compared to non-responders (ROC AUC 0.8-0.9 in post-treatment samples R vs NR; GSE18606). Finally, in a study[15] in which the intervention was a combination of IVIG with the intravenous methylprednisolone (IVMP), both ViP signatures were reduced post-Rx (ROC AUC 0.9; GSE16797), and the signatures performed equally well in both pre-treatment and post-treatment samples in differentiating responders from non-responders (ROC AUC 0.7-0.8). These findings suggest that while the IVIG-IVMP combination regimen reduced the signatures effectively among all patients (n = 17), responders induced the ViP

signatures to a lesser extent than non-responders. The 20-gene sViP signature consistently outperformed the 166-gene ViP signature in its ability to classify samples across all cohorts tested (**Figure 1C**).

We next confirmed that both the ViP signatures are induced in acute KD compared to convalescent KD in a large new cohort of consecutive patients (n=105) who were diagnosed with the disease prior to the onset of the COVID-19 pandemic (Cohort 1; **Supplementary Table 1**) (**Figure 1D**). Again, the sViP signature outperformed the ViP signature in sample classification (ROC AUC 0.91 vs. 0.74). In an independent cohort (Cohort 2, n=20, **Supplementary Table 1; Figure 1E**) prospectively enrolled in the current study after the onset of the COVID-19 pandemic, the ViP signatures could differentiate the acute from subacute KD samples. As before, the 20-gene sViP signature outperformed the 166-gene ViP signature.

Finally, we tested the association between sViP signatures and markers of disease severity. Because CAA diameter is a predictor of coronary sequelae (thrombosis, stenosis, and obstruction)[22,23] and subsequent major adverse cardiac events (unstable angina, myocardial infarction, and death[19]), we used the development of coronary artery aneurysms (CAA) as a marker of disease severity. We found that both ViP signatures differentiated acute KD with giant CAAs (defined as a z-score of ≥10 or a diameter of ≥8 mm[19,20]) from convalescent KD samples (ROC AUC 0.95 and 0.97 for ViP/sViP signatures, respectively; **Figure 1F**). Such an analysis was not possible in Cohort #2 (**Supplementary Table 1**;) because of the smaller cohort size and absence of subjects with giant CAAs.

We conclude that ViP signatures are induced in acute KD like that seen in COVID-19[12]. Because ViP signatures represent the host immune response to diverse pathogens (**Figure 1B**), upregulation of ViP signatures in KD is consistent with the hypothesis that KD is triggered by multiple infectious triggers [7,21,22], some of which may be viral in nature[23-25].

Comparison of patients with MIS-C and Kawasaki disease

Ten children were included who met the CDC definitions for MIS-C, with detectable anti-SARS-CoV-2 nucleocapsid IgG antibodies [Abbott Architect™] and undetectable virus by polymerase chain reaction (PCR; see **Figure 2**). The MIS-C and KD cohorts had notable differences. Although sex and ethnicity were not different, the median age was higher (8.8 years) in the MIS-C cohort than in KD (**Figure 2A-B**), which is in keeping with our original report describing this syndrome in June 2020[2]. Left ventricular ejection fraction (LVEF) was reduced in the MIS-C cohort ($p = 0.006$), consistent with multiple prior reports[26-28]. While all patients had evidence of a marked inflammatory state, the MIS-C cohort had significant cytopenias, including low total WBC, absolute lymphocyte, absolute eosinophil, and platelet counts, with elevation of C-reactive protein level significantly above those observed in the KD cohort (**Figure 2B**). Most patients (90%) received intravenous immunoglobulin (IVIG)

and 70% were treated with intravenous corticosteroids. One patient received anakinra, and three received infliximab. All patients made a full recovery.

ViP/sViP signatures place MIS-C and KD on the same host immune continuum, but MIS-C as farther along the spectrum than KD.

We next analyzed whole blood-derived transcriptome and serum cytokine arrays in the current cohort of subjects with KD (Cohorts 2 and 4) and MIS-C (**Figure 3A**). Both ViP (**Figure 3B**) and sViP (**Figure 3C**) signatures were induced at significantly higher levels in MIS-C samples compared to acute KD. Heatmaps of patterns of expression (**Figure 3D-E**) demonstrate that most of the individual genes contributed to the elevated ViP and sViP signatures observed in MIS-C samples. These genes included IL15 and IL15RA (highlighted in red; **Figure 3D**), both components within an invariant cytokine pathway that was previously demonstrated to be elevated in the lungs of patients with fatal COVID-19 and in SARS-CoV-2 challenged hamsters[12].

Taken together, these analyses led to two key conclusions: (i) that the host immune response, as detected in a qualitative manner using the ViP signatures, is similar in KD and MIS-C and has a IL15/IL15RA invariant component; (ii) that the degree of such host immune response, as measured quantitatively using the ViP signature scores, is more intense in MIS-C than KD. These findings are consistent with the fact that MIS-C is a host immune response to SARS-CoV-2 exposure, and we previously showed that the interaction of viral spike protein with the host entry receptor, ACE2 is critical for the induction of ViP signatures[12].

A KD-specific signature independently confirms that KD and MIS-C are syndromes on the same host immune response continuum. To circumvent an over-reliance on one set of signatures (i.e., ViP/sViP), we next analyzed a KD-specific 13 transcript signature[29] that was previously shown to be effective in distinguishing children with KD from all other febrile conditions. During validation, the 13-transcript signature mirrored the certainty of clinical diagnosis, i.e., it differentiated definite, highly probable, and possible KD from non-KD with ROC AUCs of 98.1% (95% CI, 94.5%-100%), 96.3% (95% CI, 93.3%-99.4%), and 70.0% (95% CI, 53.4%-86.6%), respectively (**Figure 3F**). Unlike the ViP signatures, which has a typical enrichment of interferon and cytokine pathways with a prominent presence of IL15/IL15RA, the KD-signature is comprised of a set of non-overlapping genes, some of which relate to major central hubs within the tumor necrosis factor (TNFα) and interleukin 6 (IL6) pathways[29]. When we applied this signature to the historic cohort (**Figure 3G**) and to our current cohort (Cohort 2; **Figure 3H**), we found that the KD-specific 13 transcript signature could not distinguish between MIS-C and KD. Furthermore, a correlation test demonstrated that the two non-overlapping signatures, sViP and KD-13, both of which are significantly induced in KD and MIS-C (**Figure 3C**) are independent of each other (**Figure S1**). The two signatures reflect two fundamentally distinct and unrelated biological domains within the host immune response, tempting us to speculate that their diagnostic/prognostic abilities may have an additive benefit.

The similar extent to which KD and MIS- C induced the signature in two independent cohorts further supports our observation with ViP/sViP signatures (**Figure 2**) that KD and MIS-C share fundamental aspects of host immune response with each other, as well as with COVID-19. All three diseases appear to be distinct clinical states on the same host immune response continuum.

Cytokine panels and whole blood transcriptomes reveal subtle differences between MIS-C and KD

We next analyzed a set of 10 serum cytokines using Meso Scale Discovery Electrochemiluminescence (MSD-ECL) Ultra-Sensitive Biomarker Assay. A panel of 10 target cytokines was prioritized based on a review of the literature for the reported presence and/or relevance of each in either KD and/or MIS-C. An unsupervised clustering of just these 10 cytokines was sufficient to differentiate acute KD and MIS-C from one-year convalescent KD samples (**Figure 4A;** Cohorts #2 and #3, **Supplementary Table 1**); the convalescent samples served as baseline 'healthy' controls in this case. Regardless of their degree of elevation in the acute setting, all cytokines were virtually undetectable in convalescent samples (**Figure S2B**). While most cytokines were induced indistinguishably in acute KD and MIS-C (**Figure 4A**; **Figure S2A**, *top*), notable exceptions were TNFα, IFNγ, IL10, IL8 and IL1β, all of which were elevated to a greater extent in MIS-C compared to KD (**Figure 4B**; **Figure S2A**, bottom), either significantly (TNFα, IFNγ; **Figure 4B**) or trended similarly, but failed to reach statistical significance (IL10, IL1β, IL8). Gene set enrichment analysis on the transcriptomic dataset for each of the differentially expressed cytokines (**Figure 4C**) showed that the gene sets for those pathways were also induced in MIS-C at levels significantly higher than KD (**Figure 4D-G**).

Taken together, these findings suggest that FDA-approved therapeutics targeting TNFα and IL1β pathways may be beneficial to treat MIS-C. The IL-1 receptor is expressed in nearly all tissues and its antagonism by anakinra, a recombinant form of IL-1Ra[30], prevents receptor binding of either IL-1α or IL-1β. Similarly, infliximab, a chimeric antibody to TNFα, has been repurposed for COVID-19[31-33], and our analyses suggest that this agent holds promise as a treatment for MIS-C.

Integrated analyses of ViP/sViP signatures, cytokine profile, and clinical laboratory parameters reveal unique features of MIS-C and indicators of disease severity. We next sought to understand how similar host cytokine responses can trigger two distinct clinical syndromes, and how such responses may drive features of clinical severity. To this end, we first carried out an agglomerative hierarchical clustering of the MIS-C and acute KD samples using both cytokine profiling (MSD) and clinical/laboratory parameters. This analysis, coupled with correlation tests (**Figure S3**) revealed several intriguing observations: (i) visualization by heatmap showed that compared to KD, MIS-C patients had higher cytokine levels and more severe pancytopenia (**Figure 5A**); (ii) although platelet counts (PLT), but not absolute eosinophil counts (AEC) were significantly reduced in MIS-C compared to KD (**Figure 5B**), there was a strong positive correlation between PLT and AEC in MIS-C, but not KD (**Figure 5C**; left) and strong negative correlations of PLT with IL15 in both KD and MIS-C (**Figure 5C**; right) and with MIP1α in MIS-C, but not KD (**Figure 5D**); (iii) this is consistent with the fact that IL15 and MIP1α were

found to have a strong positive correlation in MIS-C, but not KD (**Figure 5E**). These findings suggest that MIS-C has key distinguishing features of thrombocytopenia and low eosinophil counts, and that both features are negatively correlated with the serum levels of IL15, a key invariant feature of the ViP signature. These findings also held true when we analyzed the two clinical parameters, PLT and AEC, against ViP/sViP signatures, as well as a specific IL15/IL15RA composite transcript score from whole blood RNA Seq dataset. We found that PLT and AEC negatively correlated with ViP (**Figure 5F**; top), sViP (**Figure 5F**; middle) and a IL15/IL15RA composite score (**Figure 5F**; bottom) in MIS-C, but such correlations were restricted only to PLT in acute KD. These findings indicate that MIS-C, but not KD, has at least two distinct and interrelated clinical features, thrombocytopenia and eosinopenia, that appear to be related to the degree of induction of ViP signatures and a IL15-predominant cytokine induction. Findings also suggest that MIP1α is a key contributor to the immune response in MIS-C and that its levels are closely and positively related to the levels of IL15.

These findings reveal key similarities and differences among MIS-C, KD and COVID-19. Thrombocytopenia, which was more pronounced in MIS-C and correlated significantly with IL15 and IL15/IL15 composite transcript score in both KD and MIS-C, has also been reported in COVID-19 and postulated because of various mechanisms[34-38]. In the case of KD, thrombocytopenia has been found to be associated with disease severity[40]. Similarly, in the case of COVID-19, a large meta-analysis confirmed that approximately 12% of hospitalized patients have thrombocytopenia, which represents a sign of disease severity and poor outcomes[34]. Thrombocytopenia carried a 3-fold enhanced risk of a composite outcome of intensive care unit admission, progression to acute respiratory distress syndrome, and mortality (odds ratio [OR], 3.49; 95% CI, 1.57–7.78), and a subgroup analysis confirmed a significant association with mortality (OR, 7.37; 95% CI, 2.08–26.14). Eosinopenia appears to be a notable shared feature between MIS-C and COVID-19[41], but not KD. As in the case of thrombocytopenia, persistent eosinopenia after admission correlated with COVID-19 severity and low rates of recovery[41].

ViP/sViP signatures track the severity of two distinct cardiac phenotypes in MIS-C and KD.

We next analyzed the relationship between ViP signatures and the prominent and unique cardiac phenotype in MIS-C reported by others[26-28] and observed also in our cohort (**Figure 6A**), i.e., a significantly reduced LVEF that can present with cardiogenic shock necessitating ionotropic support. We found that sViP signature scores, but not ViP or IL15/IL15RA composite scores correlate significantly with LVEF (**Figure 6B-D**), indicating that LVEF may belong to the domain of clinical indicators of disease severity in MIS-C (alongside platelets and AEC), but it may not be directly related to the IL15-centric cytokine signaling. In KD, the ViP and sViP signatures were tested earlier (**Figure 1F**) and found to distinguish patients with giant CAA from convalescent samples with ROC AUC > 0.95. A IL15/IL15RA composite score performed similarly in distinguishing those samples (**Figure 6E**). We hypothesized that the ViP signatures may be related to two distinct cardiac phenotypes in severe disease: the signatures in KD may signify the nature of the vasculitis that drives the formation of CAAs, whereas the same signature in MIS-C may signify the degree of cardiomyopathy that impairs contractility (**Figure 6F**). Because we were unable to acquire cardiac tissues from MIS-C-related autopsies, we carried out immunohistochemical

analyses on cardiac tissues from a case of fatal KD. We found that both IL15 and IL15RA were expressed in the cardiomyocytes and coronary arterioles amidst extensive fibrosis, as detected using Masson's trichrome stain (**Figure 6G**).

Together, these findings suggest that the IL15/IL15RA induction we see in COVID-19, KD and MIS-C may have distinct sources and/or target end organs: We previously showed prominent induction of IL15/IL15RA in the lung alveoli of fatal COVID-19 patients[12], and here we show it in the coronary arteries and cardiomyocytes in KD. Because cardiomyopathy and enteropathy are the commonest presenting features of MIS-C, it is tempting to speculate that cardiac muscle and various regions of the gastrointestinal tract may be the site of IL15/IL15RA induction in MIS-C.

SUMMARY AND CONCLUSIONS

Using a combination of publicly available KD datasets and newly recruited cohorts of KD and MIS-C subjects (summarized in **Figure 7A**) and a set of gene signatures we report an unexpected discovery regarding the host immune response in these diagnoses. Our findings show that two distinct clinical syndromes, KD, which predates the current pandemic by 6 decades, and the novel COVID-19, share a similar profile of host immune response. The same host immune response is seen also in MIS-C, a new disease that co-emerged with COVID-19, which has some overlapping features with KD (i.e., clinical presentation, pediatric, etc.), and yet is an immune response to the virus that causes COVID-19 (**Figure 7B-C**). We assessed the quality and intensity of the host immune response in these syndromes with a powerful and unbiased computational tool, the ViP signatures[12]. Previously we had demonstrated the usefulness of the ViP signatures to define and measure the host immune response in COVID-19, identify the site/source of the cytokine storm, track disease severity, objectively formulate therapeutic goals and track the effectiveness of emerging drugs/biologics[12]. We now show that the same ViP signatures can objectively demonstrate the shared immunophenotypes between all three syndromes, which features an invariant upregulation of the IL15/IL15RA pathway. That a 13 transcript KD-specific signature that was previously shown to distinguish KD from other non-KD febrile illnesses[29] failed to distinguish KD from MIS-C, further confirmed that KD and MIS-C share identical molecular markers of disease and hence, are fundamentally similar at the molecular level (summarized in **Figure 7B**).

Despite the high-level broad similarities, the ViP signatures also helped identify key differences in clinical/laboratory parameters that may help distinguish MIS-C from KD. First, although the ViP signatures placed KD and MIS-C on the same host immune continuum, the degree of host immune response in MIS-C is significantly higher than KD. Higher ViP signatures in MIS-C tracked three major clinical and/or laboratory parameters (see **Figure 7B**): (i) degree of thrombocytopenia in severe cases (all three diseases), (ii) eosinopenia (in COVID-19 and MIS-C, but not KD) and (iii) impaired cardiac contractility (unique to MIS-C, but not KD). An integrated analysis of serum cytokines and transcriptomics revealed that the proinflammatory MIP1α, TNFα and IL1 pathways are significantly induced in MIS-C compared to KD. In light of these findings, a rational approach

to MIS-C treatment would be to combine the FDA-approved drugs anakinra[30] and infliximab[31-33]. In fact, during the preparation of this manuscript a new study has already shown favorable outcome in MIS-C with the use of Infliximab[43].

Finally, our findings reveal a pattern of MIS-C-defining molecular features (IL15/IL15RA, MIP1α, TNFα and IL1 pathways) and clinical and laboratory parameters (thrombocytopenia, eosinopenia, and reduced myocardial function). IL15/IL15RA, eosinopenia and thrombocytopenia may be inter-related phenomena in the setting of infection and inflammation (**Figure 7C**). Platelets, besides their role in hemostasis, they are known to participate in the interaction between pathogens and host defense[46-48]. Persistent thrombocytopenia carried higher mortality in sepsis[42,43], and in COVID-19[44,45]. Our analysis revealed a direct and unusually strong correlation between thrombocytopenia and eosinopenia in MIS-C. Eosinophils, on the other hand, as reviewed elsewhere[51], have important antiviral properties, attributed to their granular proteins (e.g., eosinophil-derived neurotoxin, cationic protein) that display antiviral activities against single-stranded RNA viruses. Eosinophils can also support viral clearance[52]. Eosinopenia, in the setting of acute infection, has been found to be a direct response to infectious stimuli[53], TLR4 ligands and chemotactic factors[54], and has been considered a reliable diagnostic marker of infection[55] in critically ill patients and a predictor of mortality[53-55]. It is possible that the two related clinical/laboratory parameters (low PLT and AEC) may be useful indicators of disease severity and prognosis in MIS-C and may guide decision-making in therapy and level of care in the hospital setting.

AUTHOR CONTRIBUTIONS

Role	Authors
Conceptualization; Supervision; Project administration • Conceptualization (PG, JCB, DS) • Supervision (PG, JCB, SD, DS) • Project Administration (PG)	PG, JCB, DS, and SD
Investigation; Methodology; Data curation, Formal Analysis • Cohort 1- KD patient recruitment and RNA seq studies (JCB, ATH) • Cohort 2 and 3- KD and MIS-C patient recruitment and collection of patient-derived samples (CS, ATH, JoKa, JB, JCB, Pediatric Emergency Medicine Kawasaki Disease Research Group*) • Serum cytokine analysis (GDK, CS, SD) • Tissue analysis (IHC)- (SK) • Computational modeling and analysis (DS) • Management of transcriptomic datasets and uploading to NCBI (JiKi)	GDK, CS, ATH, JoKa, JB, JiKi, SK, DS, JCB
Funding acquisition	DS, JCB, SD, PG
Software	DS
Visualization; Writing • Original draft (PG, GDK, C.S) • Writing – review & editing (DS, GDK, AH, JoKa, CS, JCB)	DS, GDK, CS, JoKa, AH, JCB, PG

*A list of members of the "*Pediatric Emergency Medicine Kawasaki Disease Research Group*":

- Naomi Abe, MD
- Amy Bryl, MD
- J. Joelle Donofrio-Ödmann, DO
- Atim Ekpenyong, MD
- Michael Gardiner, MD
- David J. Gutglass, MD, MBI
- Jim R. Harley, MD, MPH,
- Margaret B. Nguyen, MD
- Kristy Schwartz, MD
- Stacey Ulrich, MD

ACKNOWLEDGEMENTS

This work was supported by the National Institutes for Health (NIH) grants R01-GM138385 (to DS), R01-AI141630 (to P.G), R01DK107585 (to S.D) and R01-AI155696 (to P.G, D.S and S.D), UCOP-RGPO (R01RG3780, R00RG2628 & R00RG2642 to P.G, D.S and S.D), iDASH U54HL108460, R01HL140898 (to JCB and AHT), and a UC San Diego Stem Cell Center Pilot award (to P.G, D.S and S.D). G.D.K was supported through The American Association of Immunologists Intersect Fellowship Program for Computational Scientists and Immunologists. Clinical sample collection was supported by the Patient Outcomes Research Institute (PCORI) CER-1602-3447 (to JCB), a Gordon and Marilyn Macklin Foundation grant (JCB), and a UC San Diego Stem Cell Center Pilot award (to P.G, D.S and S.D). This publication includes data generated at the UC San Diego IGM Genomics Center Utilizing an Illumina NOVASeq 6000 that was purchased with funding from a National Institutes of Health SIG grant (#S10 OD026929).

Data and materials availability:

All data is available in the main text or the supplementary materials. RNA Seq datasets have been deposited at NCBI GEO. The GEO datasets will be embargoed for one year after publication and released to readers upon request to the corresponding authors. Source code of the software is available at https://github.com/sahoo00/BoNE and https://github.com/sahoo00/Hegemon.

FIGURE LEGENDS

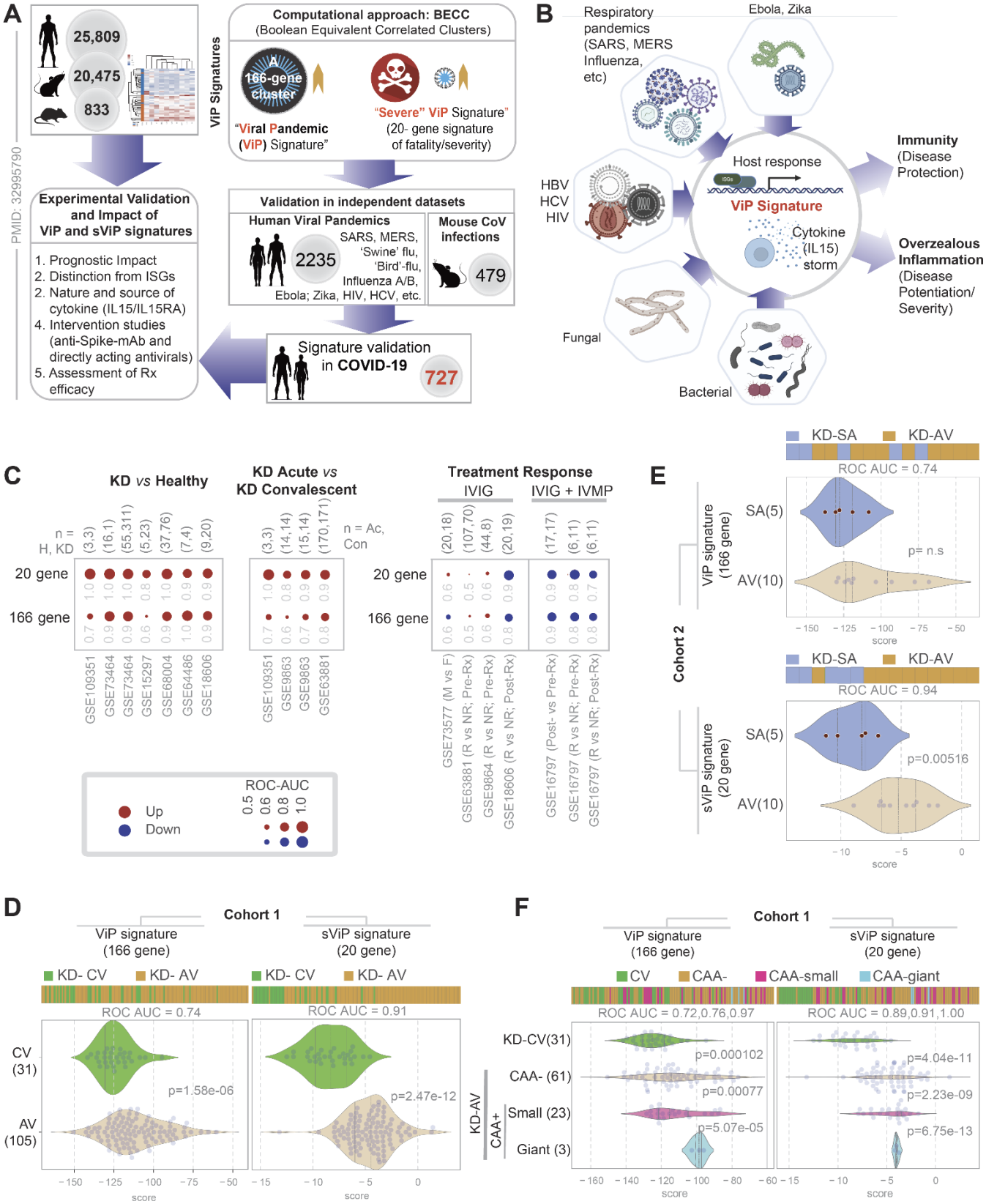

Figure 1: **A *Viral Pandemic* (ViP) signature that is induced in COVID-19[12], is induced also in epidemic outbreaks of KD**. **A**. Schematic displays the computational approach (BECC) and rigor (diversity and number

of datasets) used to identify the 166-gene ViP and a subset of 20-gene severe (s)ViP signatures, and the subsequent experimentally validated inferences and impact of the same in a recent study[12]. The numbers in grey circles denote the total number of datasets analyzed in each category. **B**. Schematic displays the various pathogenic triggers that induce ViP signatures (many of which are triggers also for KD) and the prominent induction of IL15/IL15RA as an invariant nature of the cytokine storm. **C**. Bubble plots of ROC-AUC values (radii of circles are based on the ROC-AUC) demonstrating the direction of gene regulation (Up, red; Down, blue) for the classification based on the 20-gene severe ViP signature (top) and 166-gene ViP signature (bottom) in numerous publicly available historic datasets. ViP signatures classified KD *vs*. healthy children (left), acute *vs*. convalescent KD (middle) and treatment response in the setting of combination therapy with IV steroids (MP, methylprednisone) and IV IgG alone (IVIG), but not IVIG alone. Numbers on top of bubble plots indicate number of subjects in each comparison group. **D-E**. Bar (top) and violin (bottom) plots display the classification of blood samples that were collected during acute (AV), sub-acute (SA; ~10-14 d post-discharge) and convalescent (CV; 1 y post-onset) visits from two independent KD cohorts (**D**; Historic Cohort 1**, GSEID pending; E**; Prospective Cohort 2, **GSEID pending**) using ViP (left) or sViP (right) signatures. **F**. Bar (top) and violin (bottom) plots display the sub-classification of blood samples in Cohort 1 based on coronary artery aneurysm (CAA) status using ViP (left) or sViP (right) signatures. Welch's two sample unpaired t-test is performed on the composite gene signature score to compute the p values. In multi-group setting each group is compared to the first control group and only significant p values are displayed.

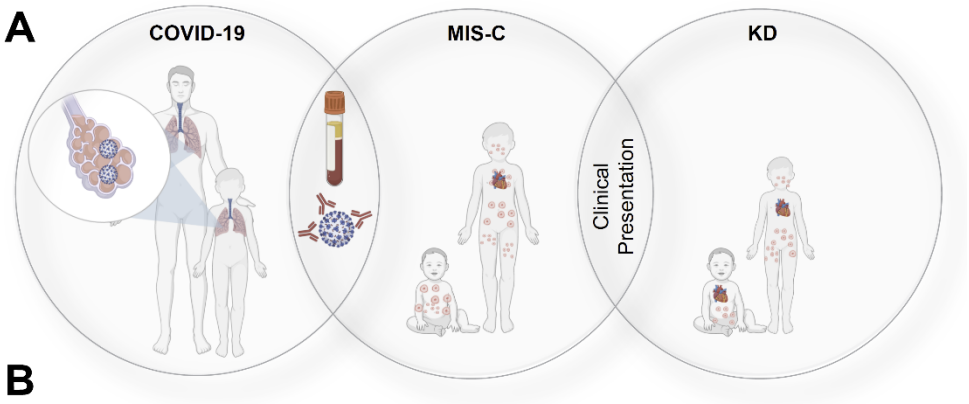

Demographic and Clinical parameters	KD		MIS-C	p-value
	CAA- (n=10)	CAA+ (n=10)	MIS-C (n=10)	
Age, yrs*	2.2 (1.8-3.7)	1.8 (1.2-3.5)	8.8 (5.7-11.1)	0.0002
Illness day**	6 (5-7)	6 (5-7)	4 (3-4)	NS
Male, n (%)	6 (60)	8 (80)	6 (60)	NS
Ethnicity, n (%)				
Asian	1 (10)	1 (10)	0	NS
African American	1 (10)	1 (10)	2 (20)	
White	3 (30)	2 (20)	1 (10)	
Hispanic	4 (40)	3 (30)	6 (60)	
> 2 races	2 (20)	5 (50)	1 (10)	
Zmax	1.0 (0.7-1.2)	3.1 (2.7-3.3)	1.9 (1.5-2.2)	0.0002
LVEF, median (IQR, range)	67 (65-68, 56-76)	70 (62-75, 56-79)	58 (55-62, 31-65)	0.006
Laboratory data				
WBC, 10^3/ µL	12.6 (11.6-18.3)	15.8 (13.0-18.5)	11.1 (5.5-11.7)	0.01
ANC, / µL	9159 (6904-106830	11319 (8896-12539)	8172 (4437-10071)	NS
ALC, /µL	2576 (1739-3658)	2924 (2379-5075)	939 (803-1019)	0.0002
AEC, /µL	184 (104-529)	378 (322-588)	122 (0-231)	0.04
ZHgb	-1.4 (-2.3-0.1)	-1.5 (-1.8--0.6)	-2.2 (-2.7--0.7)	NS
PLT, 10^3/mm^3	330 (278-396)	363 (338-396)	177 (106-228)	0.002
ESR, mm/h	55 (30-64)	68 (58-76)	44 (36-59)	NS
CRP, mg/dL	6.1 (4.8-12.2)	5.9 (4.0-8.0)	21 (19.6-23.8)	0.01
BNP, pg/mL	ND	ND	33 (19.7-23.6)	NA
Ferritin, ng/mL	ND	ND	323 (223-960)	NA
Troponin, ng/mL	ND	ND	0.02 (0.01-0.13)	NA
D-dimer, µg/mL	ND	ND	1.94 (1.24-2.40)	NA
SARS-CoV-2 testing				
PCR positive	ND	ND	1 (10)	NA
IgG positive***	ND	ND	10 (100)	NA
Treatment/ n (%)				
IVIG x1	10 (100)	10 (100)	8 (80)	NS
IVIG x2	0	1 (10)	1 (10)	NS
Infliximab	4 (40)	10 (100)	3 (30)	0.003
Anakinra	0	1 (10)	1 (10)	NS
Cyclosporine	0	1 (10)	0	NS
Corticosteroids	0	0	7 (70)	0.0001

Figure 2: **Characteristics of patients with Kawasaki disease (KD) and MIS-C analyzed in this study**.

A. Schematic displays the current understanding of what are the unique and overlapping features of the three clinical presentations: COVID-19, MIS-C and Kawasaki disease. **B.** Table displays the demographic, clinical and laboratory parameters collected on the KD and patients with MISC-C enrolled into the study. *: median (Interquartile range (IQR) unless specified. **Illness Day 1= first day of fever. *** SARS-CoV-2 nucleocapsid IgG positive n=9 and SARS-CoV-2 peptide array n=1. Zmax: Maximum Z score (internal diameter normalized for body surface area) for the right and left anterior descending coronary arteries. Laboratory data are pre-treatment. Troponin was measured in nine patients with MIS-C. D-dimer was measured in eight patients with MIS-C. Abbreviations: LVEF: left ventricular ejection fraction, WBC: white blood cell count, PLT, platelets; AEC, absolute eosinophil count; ANC: absolute neutrophil count, ALC: absolute lymphocyte count, CRP: C-reactive protein, ESR: erythrocyte sedimentation rate, BNP: brain natriuretic peptide, ZHgb: hemoglobin concentration normalized for age. NS: not significant, NA: not applicable, ND: not done, p-values were calculated by Kruskal-Wallis test for continuous variables among three groups and Chi-test for categorical variables.

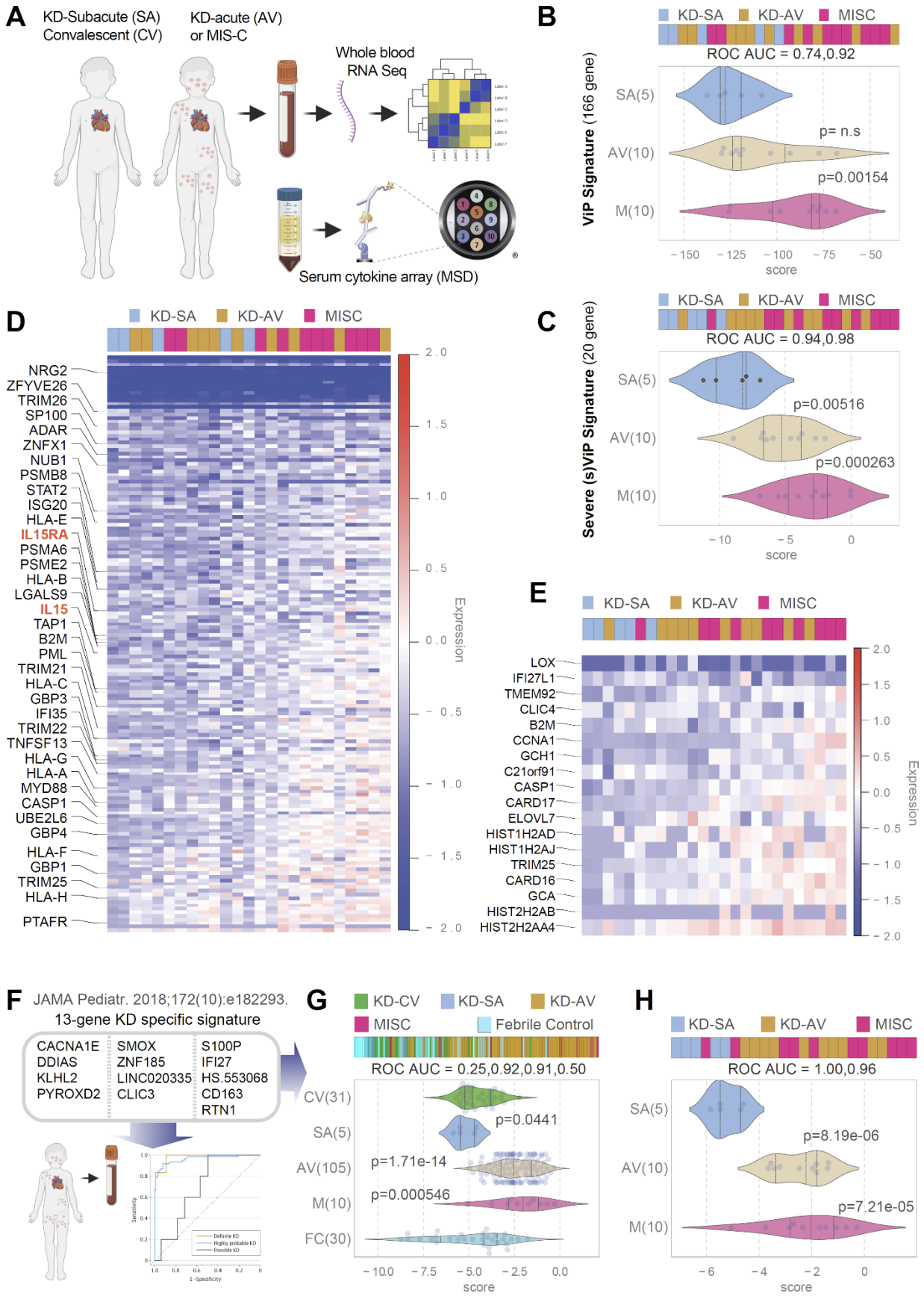

Figure 3. A KD-specific 13 transcript signature[29] shows that KD and MIS-C are indistinguishable, but ViP/sViP signatures place MIS-C as farther along the spectrum than KD. A. Schematic displays the workflow

for patient blood collection and analysis by RNA Seq (this figure) and cytokine array by mesoscale (**Figure 4-5**). **B-C**. Bar (top) and violin (bottom) plots display the classification of blood samples that were collected during collected during acute (AV) and sub-acute (SA; ~10-14 d post-discharge) visits of KD subjects and from patients diagnosed with MIS-C. **D-E**. Heatmaps display the patterns of expression of the 166 genes in ViP (D) and 20 gene sViP (E) signatures in the KD and MIS-C samples. The only cytokine-receptor pair within the signature, i.e., IL15/IL15RA, are highlighted on the left in red font in D. **F**. Schematic displays the 13- transcript whole blood signature (no overlaps with ViP signature genes) previously demonstrated to distinguish KD from other childhood febrile illnesses[29]. **G-H**. Bar (top) and violin (bottom) plots display the classification of blood samples that were collected during acute (AV) and convalescent (CV) visits from two independent KD cohorts (**G**; Historic Cohort 1**, GSEID pending; E**; Prospective Cohort 2, **GSEID pending**) using 13-transcript KD signature. FC, febrile control. See also **Figure S1** for co-dependence analysis of ViP and KD-13 signatures. Welch's two sample unpaired t-test is performed on the composite gene signature score to compute the p values. In multi-group setting each group is compared to the first control group and only significant p values are displayed.

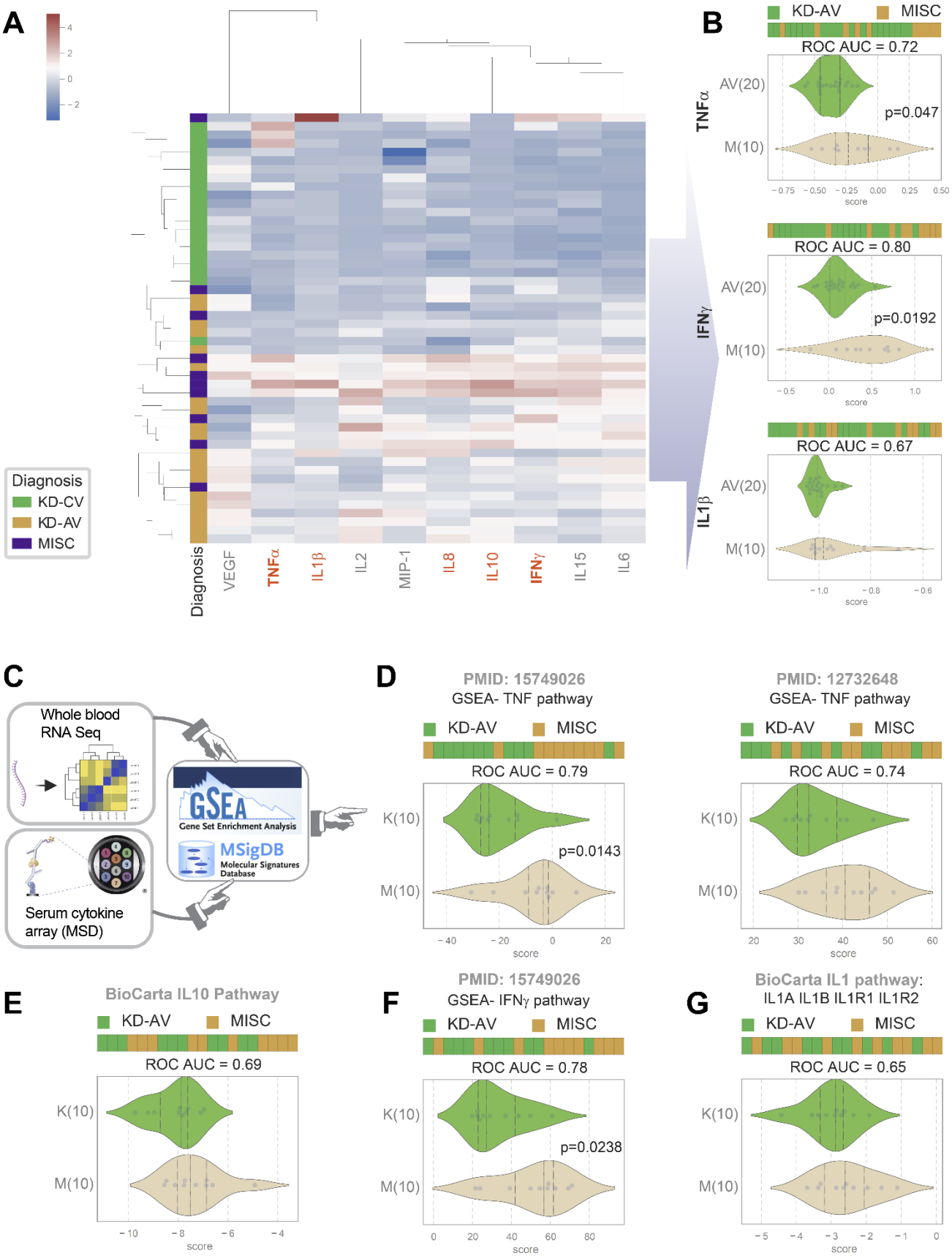

Figure 4: Serum cytokine arrays and whole blood transcriptomes reveal the severity and nature of the cytokine storm in MIS-C that distinguishes it from KD. A. Heatmap displays the results of unsupervised

clustering of sub-acute and acute KD (KD-SA, KD-AV; n = 10 each) and MIS-C (n = 10) subjects using the cytokine profiles determined by mesoscale (MSD). Red = cytokines differentially expressed between MIS-C and KD. See also **Figure S2** for violin plots for individual cytokines. **B**. Bar (top) and violin (bottom) plots for the cytokines that are differentially induced between KD and MIS-C. ROC AUC numbers indicate the strength of classification in each instance. **C**. Schematic shows the process used to integrate serum cytokine array results with whole blood RNA Seq data; cytokines that were differentially expressed in MIS-C were used to inform GSEA of the corresponding pathways. **D-G**. Bar (top) and violin (bottom) plots show that for each cytokine that was found to be differentially expressed in cytokine array were associated with a corresponding induction of genes within the cytokine pathways by RNA Seq. Welch's two sample unpaired t-test is performed on the composite gene signature score to compute the p values.

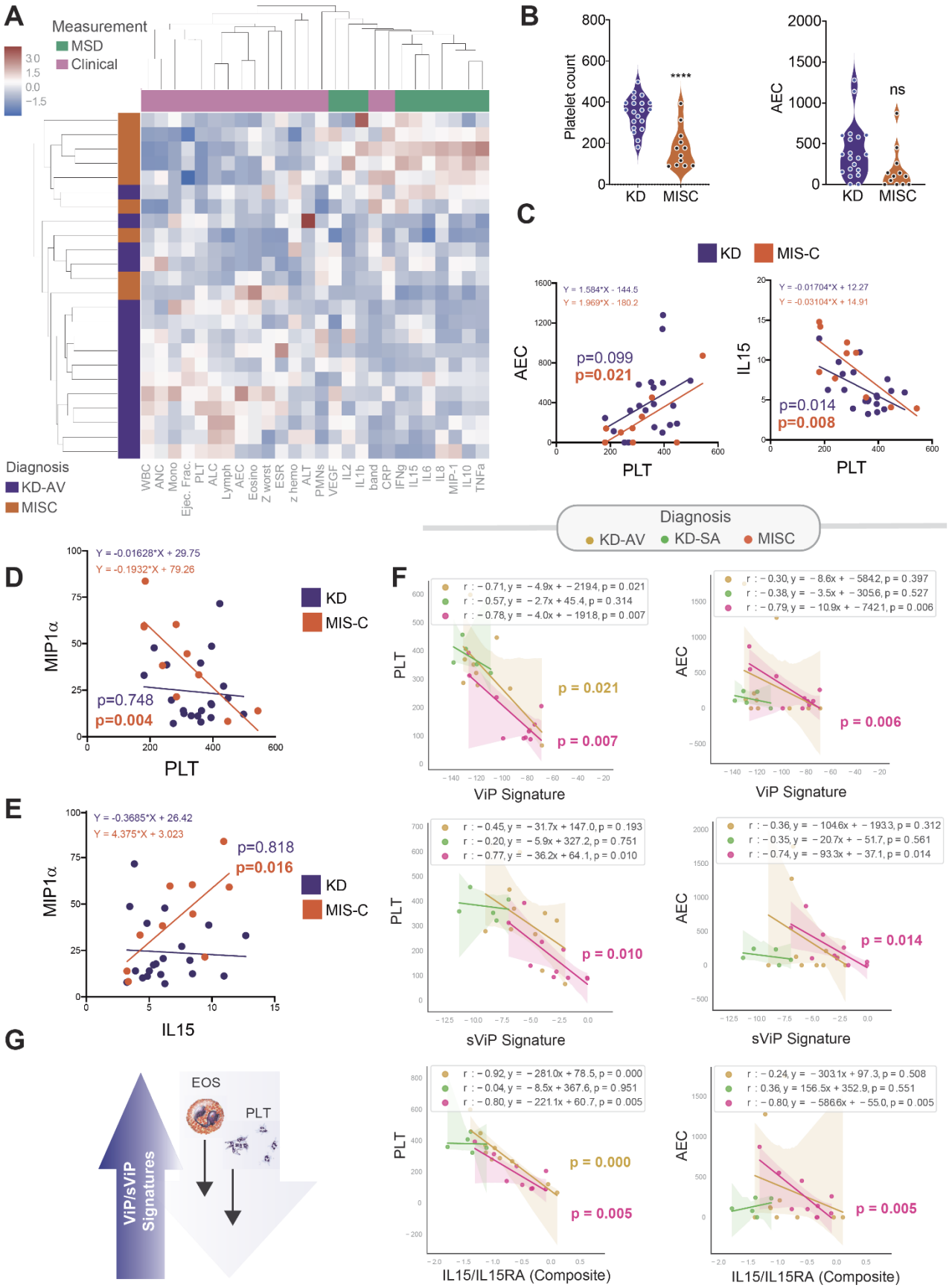

Figure 5: **An integrated analysis of mesoscale (cytokine) data, ViP/sViP transcriptomic signatures and laboratory and clinical parameters reveals features that are unique to MIS-C**. **A**. Heatmap displays the

results of hierarchical agglomerative clustering of acute KD (KD-AV; n = 10) and MIS-C (n = 10) subjects using the cytokine profiles determined by mesoscale (MSD) and the laboratory features. **B**. Violin plots display PLT (platelet) and AEC (absolute eosinophil counts) in KD and MIS-C (Student's t-test used to test significance). **C-E**. Correlation test between AEC and PLT (C; left) and IL15 and PLT (C; right), and MIP1α and PLT (D) and MIP1α and IL15 (E) are shown and significance was calculated and displayed using GraphPad Prism 9. Significance: ns: non-significant, ****, $p < 0.0001$. See **Figure S3** for all possible correlation tests between clinical and cytokine data in KD, MIS-C and COVID-19. **F**. Correlation tests between PLT (left) or AEC (right) on the Y axis and gene signature scores on the X axis [either ViP (top), sViP (middle) or a IL15/IL15RA composite (bottom)] were calculated and displayed as scatter plots using python seaborn lmplots with the p-values. The confidence interval around the regression line is indicated with shades. **G**. Schematic summarizing the findings in MIS-C based on laboratory and RNA seq analysis.

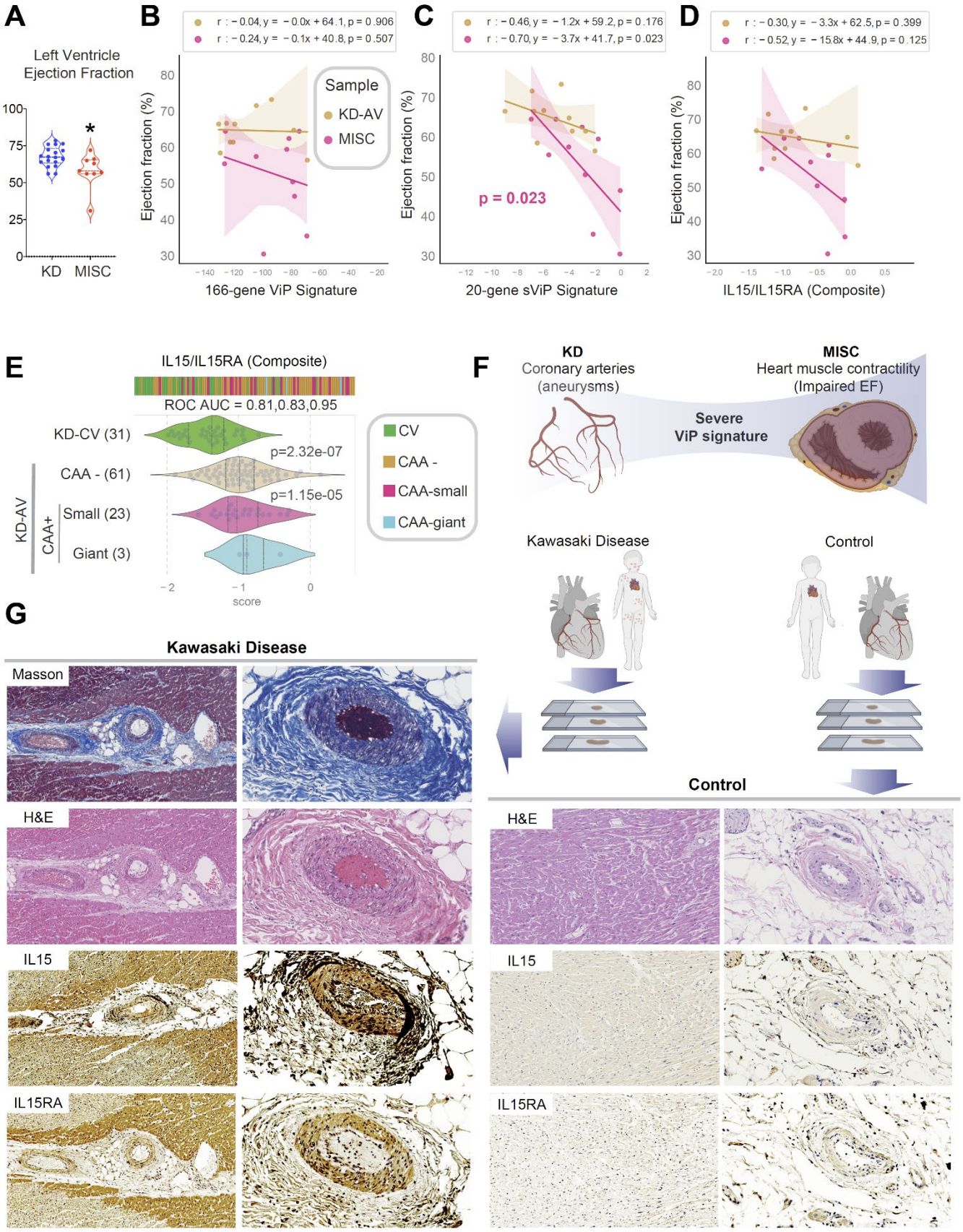

Figure 6: **ViP/sViP signatures correlate with two distinct cardiac phenotypes in MIS-C and KD.**

A. Violin plots display the left ventricular ejection functions (LVEF) in KD and MIS-C patients. Significance was determined by t-test; * = $p < 0.05$. **B-D**. Correlation tests between LVEF (Y axis) and gene signature scores on the X axis [either ViP (B), sViP (C) or a IL15/IL15RA composite (D)] are displayed as a scatter plot and significance was calculated and displayed as in **5F**. The confidence interval around the regression line is indicated with shades. **E**. Bar and violin plots show how a IL15/IL15RA compositive score varies between KD samples. The score classifies KD-AV with giant CAAs from control (KD-CV) samples with a ROC AUC 0.95. Welch's two sample unpaired t-test is performed on the composite gene signature score to compute the p values. In multi-group setting each group is compared to the first control group and only significant p values are displayed. **F**. Schematic summarizes how sViP signature classifies two distinct cardiac phenotypes, CAA and reduced pump function in KD and MIS-C, respectively. **G**. Consecutive sections from formalin fixed paraffin-embedded (FFPE) cardiac tissue collected at autopsy from a child with severe debilitating cardiac complications of KD were stained for masson's trichrome, H&E and IL15/IL15RA antigens (left). Healthy heart sections from another child were used as controls (right).

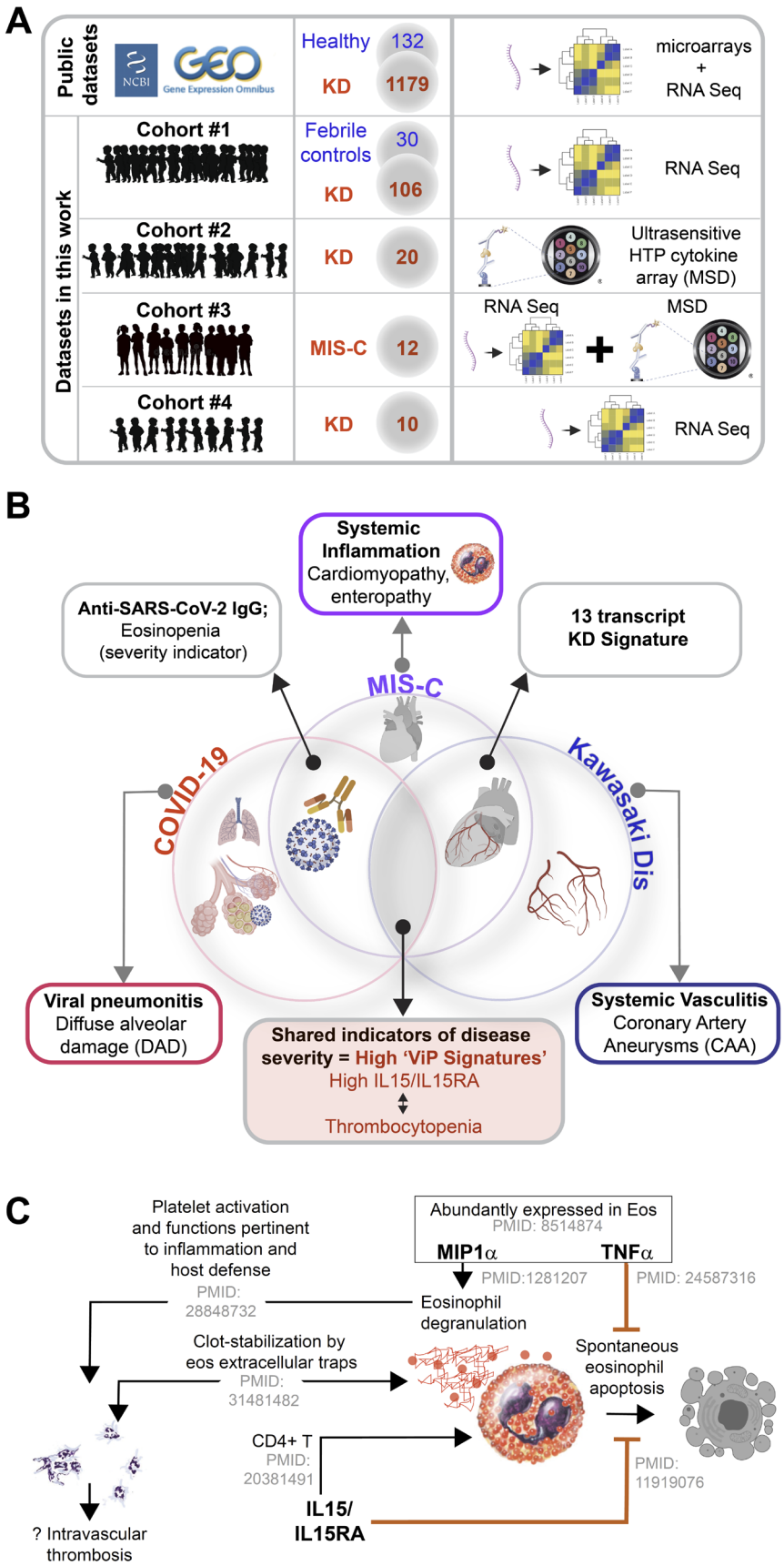

Figure 7. **Summary of findings and conclusions**. **A.** Summary of datasets used (publicly available prior ones and new original cohorts) to support the conclusions in this work. Numbers in circles denote the number of

subjects in each cohort. **B.** Venn diagram displays the major findings from the current work. ViP/sViP signatures, and more specifically, the IL15/IL15RA specific gene induction are shared between patients in all three diagnostic groups. While these signatures are known to be associated with diffuse alveolar damage in the lungs of patients with COVID-19[12], it is associated with CAA in KD and with reduction in cardiac muscle contractility in MIS-C. Overlapping features between each entity are displayed. **C.**Schematic displaying the interpretation of the unique findings in MIS-C (thrombocytopenia, low eosinophil counts with concomitant increase in ViP signatures and the IL15/IL15RA pathway) in light of existing literature.

REFERENCES

1. Levin, M. Childhood Multisystem Inflammatory Syndrome - A New Challenge in the Pandemic. *N Engl J Med* **383**, 393-395 (2020).
2. Whittaker, E.*, et al.* Clinical Characteristics of 58 Children With a Pediatric Inflammatory Multisystem Syndrome Temporally Associated With SARS-CoV-2. *Jama* **324**, 259-269 (2020).
3. Riphagen, S., Gomez, X., Gonzalez-Martinez, C., Wilkinson, N. & Theocharis, P. Hyperinflammatory shock in children during COVID-19 pandemic. *Lancet* **395**, 1607-1608 (2020).
4. Toubiana, J.*, et al.* Kawasaki-like multisystem inflammatory syndrome in children during the covid-19 pandemic in Paris, France: prospective observational study. *Bmj* **369**, m2094 (2020).
5. Kawasaki, T., Kosaki, F., Okawa, S., Shigematsu, I. & Yanagawa, H. A new infantile acute febrile mucocutaneous lymph node syndrome (MLNS) prevailing in Japan. *Pediatrics* **54**, 271-276 (1974).
6. Makino, N.*, et al.* Descriptive epidemiology of Kawasaki disease in Japan, 2011-2012: from the results of the 22nd nationwide survey. *J Epidemiol* **25**, 239-245 (2015).
7. Nakamura, A., Ikeda, K. & Hamaoka, K. Aetiological Significance of Infectious Stimuli in Kawasaki Disease. *Frontiers in Pediatrics* **7**(2019).
8. Manlhiot, C.*, et al.* Environmental epidemiology of Kawasaki disease: Linking disease etiology, pathogenesis and global distribution. *PLoS One* **13**, e0191087 (2018).
9. Rodó, X.*, et al.* Tropospheric winds from northeastern China carry the etiologic agent of Kawasaki disease from its source to Japan. *Proceedings of the National Academy of Sciences*, 201400380 (2014).
10. Dufort, E.M.*, et al.* Multisystem Inflammatory Syndrome in Children in New York State. *N Engl J Med* **383**, 347-358 (2020).
11. Sahoo, D.*, et al.* AI-guided discovery of the invariant host response to viral pandemics. *bioRxiv* (2020).
12. Tai, W.*, et al.* Characterization of the receptor-binding domain (RBD) of 2019 novel coronavirus: implication for development of RBD protein as a viral attachment inhibitor and vaccine. *Cell Mol Immunol* **17**, 613-620 (2020).
13. Hoffmann, M.*, et al.* SARS-CoV-2 Cell Entry Depends on ACE2 and TMPRSS2 and Is Blocked by a Clinically Proven Protease Inhibitor. *Cell* **181**, 271-280.e278 (2020).
14. Dabydeen, S.A., Desai, A. & Sahoo, D. Unbiased Boolean analysis of public gene expression data for cell cycle gene identification. *Mol Biol Cell* **30**, 1770-1779 (2019).
15. Ogata, S.*, et al.* Clinical score and transcript abundance patterns identify Kawasaki disease patients who may benefit from addition of methylprednisolone. *Pediatr Res* **66**, 577-584 (2009).
16. Yanagawa, H.*, et al.* Update of the epidemiology of Kawasaki disease in Japan--from the results of 1993-94 nationwide survey. *J Epidemiol* **6**, 148-157 (1996).
17. Ben Tsutomu Saji, J.W.N. & Jane C. Burns, M.T. Guidelines for diagnosis and management of cardiovascular sequelae in Kawasaki disease (JCS 2013). Digest version. *Circ J* **78**, 2521-2562 (2014).
18. Eleftheriou, D.*, et al.* Management of Kawasaki disease. *Arch Dis Child* **99**, 74-83 (2014).
19. McCrindle, B.W.*, et al.* Coronary artery involvement in children with Kawasaki disease: risk factors from analysis of serial normalized measurements. *Circulation* **116**, 174-179 (2007).
20. Manlhiot, C., Millar, K., Golding, F. & McCrindle, B.W. Improved classification of coronary artery abnormalities based only on coronary artery z-scores after Kawasaki disease. *Pediatr Cardiol* **31**, 242-249 (2010).
21. Burns, J.C.*, et al.* Temporal Clusters of Kawasaki Disease Cases Share Distinct Phenotypes That Suggest Response to Diverse Triggers. *J Pediatr* **229**, 48-53.e41 (2021).
22. Rypdal, M.*, et al.* Clustering and climate associations of Kawasaki Disease in San Diego County suggest environmental triggers. *Sci Rep* **8**, 16140 (2018).
23. Rigante, D. Kawasaki Disease as the Immune-Mediated Echo of a Viral Infection. *Mediterr J Hematol Infect Dis* **12**, e2020039 (2020).
24. Jordan-Villegas, A., Chang, M.L., Ramilo, O. & Mejías, A. Concomitant respiratory viral infections in children with Kawasaki disease. *Pediatr Infect Dis J* **29**, 770-772 (2010).
25. Chang, L.Y.*, et al.* Viral infections associated with Kawasaki disease. *J Formos Med Assoc* **113**, 148-154 (2014).
26. Belhadjer, Z.*, et al.* Acute Heart Failure in Multisystem Inflammatory Syndrome in Children in the Context of Global SARS-CoV-2 Pandemic. *Circulation* **142**, 429-436 (2020).

27. Friedman, K.G., Harrild, D.M. & Newburger, J.W. Cardiac Dysfunction in Multisystem Inflammatory Syndrome in Children: A Call to Action. *J Am Coll Cardiol* **76**, 1962-1964 (2020).
28. Matsubara, D.*, et al.* Echocardiographic Findings in Pediatric Multisystem Inflammatory Syndrome Associated With COVID-19 in the United States. *J Am Coll Cardiol* **76**, 1947-1961 (2020).
29. Wright, V.J.*, et al.* Diagnosis of Kawasaki Disease Using a Minimal Whole-Blood Gene Expression Signature. *JAMA Pediatr* **172**, e182293 (2018).
30. Dinarello, C.A., Simon, A. & van der Meer, J.W. Treating inflammation by blocking interleukin-1 in a broad spectrum of diseases. *Nat Rev Drug Discov* **11**, 633-652 (2012).
31. Del Valle, D.M.*, et al.* An inflammatory cytokine signature predicts COVID-19 severity and survival. *Nat Med* **26**, 1636-1643 (2020).
32. Robinson, P.C.*, et al.* The Potential for Repurposing Anti-TNF as a Therapy for the Treatment of COVID-19. *Med (N Y)* **1**, 90-102 (2020).
33. Feldmann, M.*, et al.* Trials of anti-tumour necrosis factor therapy for COVID-19 are urgently needed. *Lancet* **395**, 1407-1409 (2020).
34. Zong, X., Gu, Y., Yu, H., Li, Z. & Wang, Y. Thrombocytopenia Is Associated with COVID-19 Severity and Outcome: An Updated Meta-Analysis of 5637 Patients with Multiple Outcomes. *Lab Med* **52**, 10-15 (2021).
35. Martincic, Z.*, et al.* Severe immune thrombocytopenia in a critically ill COVID-19 patient. *Int J Infect Dis* **99**, 269-271 (2020).
36. Iba, T., Levy, J.H., Levi, M. & Thachil, J. Coagulopathy in COVID-19. *J Thromb Haemost* **18**, 2103-2109 (2020).
37. Xu, P., Zhou, Q. & Xu, J. Mechanism of thrombocytopenia in COVID-19 patients. *Ann Hematol* **99**, 1205-1208 (2020).
38. Bhattacharjee, S. & Banerjee, M. Immune Thrombocytopenia Secondary to COVID-19: a Systematic Review. *SN Compr Clin Med*, 1-11 (2020).
39. Arora, K., Guleria, S., Jindal, A.K., Rawat, A. & Singh, S. Platelets in Kawasaki disease: Is this only a numbers game or something beyond? *Genes Dis* **7**, 62-66 (2020).
40. Tanni, F.*, et al.* Eosinopenia and COVID-19. *J Am Osteopath Assoc* (2020).
41. Lindsley, A.W., Schwartz, J.T. & Rothenberg, M.E. Eosinophil responses during COVID-19 infections and coronavirus vaccination. *J Allergy Clin Immunol* **146**, 1-7 (2020).
42. Venkata, C., Kashyap, R., Farmer, J.C. & Afessa, B. Thrombocytopenia in adult patients with sepsis: incidence, risk factors, and its association with clinical outcome. *J Intensive Care* **1**, 9 (2013).
43. Tsirigotis, P.*, et al.* Thrombocytopenia in critically ill patients with severe sepsis/septic shock: Prognostic value and association with a distinct serum cytokine profile. *J Crit Care* **32**, 9-15 (2016).
44. Bashash, D.*, et al.* The Prognostic Value of Thrombocytopenia in COVID-19 Patients; a Systematic Review and Meta-Analysis. *Arch Acad Emerg Med* **8**, e75 (2020).
45. Liao, D.*, et al.* Haematological characteristics and risk factors in the classification and prognosis evaluation of COVID-19: a retrospective cohort study. *Lancet Haematol* **7**, e671-e678 (2020).
46. Speth, C., Löffler, J., Krappmann, S., Lass-Flörl, C. & Rambach, G. Platelets as immune cells in infectious diseases. *Future Microbiol* **8**, 1431-1451 (2013).
47. Assinger, A. Platelets and infection - an emerging role of platelets in viral infection. *Front Immunol* **5**, 649 (2014).
48. Seyoum, M., Enawgaw, B. & Melku, M. Human blood platelets and viruses: defense mechanism and role in the removal of viral pathogens. *Thromb J* **16**, 16 (2018).
49. Jesenak, M.*, et al.* Immune Parameters and COVID-19 Infection – Associations With Clinical Severity and Disease Prognosis. *Frontiers in Cellular and Infection Microbiology* **10**(2020).
50. Jesenak, M. & Schwarze, J. Lung eosinophils-A novel "virus sink" that is defective in asthma? *Allergy* **74**, 1832-1834 (2019).
51. Bass, D.A. Reproduction of the eosinopenia of acute infection by passive transfer of a material obtained from inflammatory exudate. *Infect Immun* **15**, 410-416 (1977).
52. Bass, D.A.*, et al.* Eosinopenia of acute infection: Production of eosinopenia by chemotactic factors of acute inflammation. *J Clin Invest* **65**, 1265-1271 (1980).
53. Abidi, K.*, et al.* Eosinopenia is a reliable marker of sepsis on admission to medical intensive care units. *Crit Care* **12**, R59 (2008).

54. Shaaban, H., Daniel, S., Sison, R., Slim, J. & Perez, G. Eosinopenia: Is it a good marker of sepsis in comparison to procalcitonin and C-reactive protein levels for patients admitted to a critical care unit in an urban hospital? *J Crit Care* **25**, 570-575 (2010).
55. Abidi, K.*, et al.* Eosinopenia, an early marker of increased mortality in critically ill medical patients. *Intensive Care Med* **37**, 1136-1142 (2011).

Table 1. Characteristics of patients and cohorts.

Cohort	Cohort 1			Cohort 2				Cohort 3		Cohort 4	
Patients	KD (n=106)[*5]		Febrile control (n=30)	KD (n=20)				MIS-C (n=12)		KD (n=10)[*5]	
				CAA- (n=10)		CAA+ (n=10)[*5]					
Samples	Acute (n=105)[*6]	Late convalescent (n=31)[*6]	Acute (n=30)	Acute (n=10)	Late convalescent (n=10)	Acute (n=10)	Late convalescent (n=10)	Acute (n=12)		Acute (n=10)	Subacute (n=5)
Assay (sample number)	RNAseq (n=166)			Mesoscale (n=40)				Mesoscale (n=10)[*10]	RNAseq (n=10)[*10]	RNAseq (n=15)	
Age, yrs[*1]	3.2 (1.7-4.8)	4.2 (2.9-6.3)	3.1 (1.7-5.4)	2.2 (1.8-3.7)	3.7 (3.1-5.2)	1.8 (1.2-3.5)	3.2 (2.3-4.8)	8.8 (5.7-11.1)	10.1 (6.5-11.1)	4.7 (2.7-5.6)	4.8 (2.6-5.8)
Illness day[*2]	5 (4-7)	412 (382-477)	6 (4-8)	6 (5-7)	416 (394-522)	6 (5-7)	455 (427-508)	4 (3-4)	3.5 (3-5)	5 (5-7)	21 (19-23)
Male, n (%)	64 (61)	17 (55)	18 (60)	6 (60)		8 (80)		6 (60)	8 (80%)	4 (40)	0
Ethnicity, n (%)											
Asian	17 (16)	8 (26)	1 (3)	1 (10)		1 (10)		0	0	2 (20)	1 (20)
African American	3 (3)	0	1 (3)	1 (10)		1 (10)		2 (20)	2 (20)	0	0
White	25 (24)	5 (16)	13 (44)	3 (30)		2 (20)		1 (10)	0	2 (20)	1 (20)
Hispanic	40 (38)	8 (26)	10 (33)	4 (40)		2 (20)		6 (60)	7 (70)	5 (50)	2 (40)
> 2 races	20 (19)	10 (32)	5 (17)	2 (20)		4 (40)		1 (10)	1 (10)	1 (10)	1 (20)
Zmax[*3]	1.8 (1.2-2.5)	NA	NA	1.0 (0.7-1.2)		3.1 (2.7-3.3)		1.9 (1.5-2.2)	1.9 (1.3-2.4)	2.3 (1.3-3.1)	NA
LVEF, median (IQR, range)	68 (64-73, 55-83)	NA	NA	67 (65-68, 56-76)		70 (62-75, 56-79)		58 (55-62, 31-65)	57 (48-62, 31-65)	66 (62-67, 59-74)	NA
Lab data:											
WBC, $10^3/\mu L$	12.9 (10.2-17.0)	NA	10.0 (6.2-13.3)	12.6 (11.6-18.3)	ND	15.8 (13.0-18.5)	ND	11.1 (5.5-11.7)	8.3 (5.0-11.2)	11.6 (10.6-12.3)	8 (7.8-8.1)
ANC, /µL	9020 (6264-11232)	NA	4616 (2830-6404)	9159 (6904-106830	ND	11319 (8896-12539)	ND	8172 (4437-10071)	6252 (4301-9002)	7302 (6336-9034)	3270 (2604-4212)
ALC, /µL	2520 (1394-3740)	NA	3074 (2121-4210)	2576 (1739-3658)	ND	2924 (2379-5075)	ND	939 (803-1019)	807 (459-1007)	2142 (1527-3495)	2852 (2418-4536)
AEC, /µL	655 (480-979)	NA	0 (0-73)	184 (104-529)	ND	378 (322-588)	ND	122 (0-231)	102 (12-230)	58 (0-189)	109 (80-234)
ZHgb	-1.4 (-2.3- -0.5)	NA	-0.6 (-1.4-0.2)	-1.4 (-2.3-0.1)	ND	-1.5 (-1.8--0.6)	ND	-2.2 (-2.8- -0.7)	-2.2 (-2.8- -0.5)	-1.5 (-2.2-0.1)	-1.0 (-2.0- 0.3)
PLT, $10^3/mm^3$	342 (255-426)	NA	208 (170-284)	330 (278-396)	ND	363 (338-396)	ND	177 (106-228)	128 (92-228)	305 (270-366)	359 (353-407)
ESR, mm/h	55 (44-73)	NA	32 (1646)	55 (30-64)[*7]	ND	68 (58-76)	ND	44 (36-59)[*8]	41 (36-56)	66 (39-79)	31 (30-32)
CRP, mg/dL	7.0 (4.2-15.6)	NA	3.1 (1.3-6.3)	6.1 (4.8-12.2)	ND	5.9 (4.0-8.0)	ND	21 (19.6-23.8)	21 (20-26)	8.1 (4.8-12.5)	0.5 (0.5-0.6)
BNP, pg/mL	ND	NA	NA	ND	ND	ND	ND	33 (19.7-23.6)[*8]	114 (33-339)[*8]	ND	ND
Ferritin, ng/mL	ND	NA	NA	ND	ND	ND	ND	323 (223-960)[*8]	746 (323-1019)[*8]	ND	ND
Troponin, ng/mL	ND	NA	NA	ND	ND	ND	ND	0.02 (0.01-0.13)[*8]	0.04 (0.01-0.14)[*8]	ND	ND
D-dimer, µg/mL	ND	NA	NA	ND	ND	ND	ND	1.94 (1.24-2.40)[*9]	2.34 (1.71-3.02)[*8]	ND	ND
SARS-CoV-2 testing											
PCR positive	NA	NA	NA	NA	NA	NA	NA	1 (10)	1 (10)	NA	NA
IgG positive[*4]	NA	NA	NA	NA	NA	NA	NA	10 (100)	10 (100)	NA	NA
Treatment, n (%)											
IVIG x1	99 (94.3)	NA	NA	10 (100)	NA	10 (100)	NA	8 (80)	9 (90)	10 (100)	NA
IVIG x2	6 (5.7)	NA	NA	0	NA	1 (10)	NA	1 (10)	0		NA
Infliximab	40 (38.1)	NA	NA	4 (40)	NA	10 (100)	NA	3 (30)	4 (40)	10 (100)	NA
Anakinra	0	NA	NA	0	NA	1 (10)	NA	1 (10)	1 (10)	0	NA
Cyclosporine	2 (1.9)	NA	NA	0	NA	1 (10)	NA	0	0	0	NA
Steroids	0	NA	NA	0	NA	0	NA	7 (70)	7 (70)	0	NA

*1: median (Interquartile range (IQR)) unless specified. *2: Illness Day 1= first day of fever. *3: Zmax: Maximum Z score (internal diameter normalized for body surface area) for the right and left anterior descending coronary arteries. *4: SARS-CoV-2 IgG positive by Abbott Architecht® nucleocapsid n=10, by Ortho Clinical Diagnostics VITROS Immunodiagnostic Spike protein n=1 and SARS-CoV-2 peptide array n=1.Laboratory data are pre-treatment unless subacute clinic visit. *5: one patient overlap between Cohort 1 and Cohort 2 and one patient overlap between Cohort 2 and Cohort 4. *6: 29 pts. have acute and late convalescent paired samples. *7 ESR was available in nine CAA-KD. *8: measured in nime MIS-C. *9: D-dimer was measured in eight MIS-C in mesoscale. *10: Eight MIS-C pts overlap between mesoscale and RNAseq. Abbreviations: LVEF: left ventricular ejection fraction, WBC: white blood cell count, ANC: absolute neutrophil count, ALC: absolute lymphocyte count, AEC: absolute eosinophil count, CRP: C-reactive protein, ESR: erythrocyte sedimentation rate, BNP: brain natriuretic peptide, ZHgb: hemoglobin concentration normalized for age. NS: not significant, NA: not applicable, ND: not done

Sample	Sample Group	Sample	VEGF Calc. Conc	VEGF Signal	IL15 Calc. Conc	IL15 Signal	MIP-1α Calc. Conc. M	MIP-1α Signal	IFNg Calc. Concentra	IFNg Signal	IL10 Calc. Conc	IL10 Signal	IL1b Calc. Conc	IL1b Signal	IL2 Calc. Conc	IL2 Signal	IL6 Calc. Conc	IL6 Signal	IL8 Calc. Conc	IL8 Signal	TNFa Calc. Conc	TNFa Signal
183082 E7	1y Convalescent (CAA+)	183082 E7	97.60691	4383	2.651439	392	5.71560663	102	3.373976798	430	0.273775	324	0.019821	238	NaN	285	0.246854	208	5.403246	2257	1.348683	585
173088 E3	1y Convalescent (CAA+)	173088 E3	62.60553	2548	4.674126	646	9.78156846	123	103.34618	5291	1.186283	734	0.067881	287	0.280243	456	2.938555	695	2.886991	1284	1.606449	650
173017 B7	1y Convalescent (CAA+)	173017 B7	194.23	10300	3.481151	495	6.8804462	107	109.4467741	5588	0.550427	449	0.076718	296	0.29792	462	0.796336	300	13.44166	5410	11.58221	3214
173007 B4	1y Convalescent (CAA+)	173007 B4	60.72884	2456	1.878313	298	7.89014168	112	3.724798608	447	0.435096	397	0.090469	310	0.043756	375	0.557032	259	3.546652	1538	1.638133	658
163116 B2	1y Convalescent (CAA+)	163116 B2	31.35867	1127	3.855092	542	10.3922218	127	59.68082479	3166	4.933796	2391	0.092434	312	0.457568	516	1.153957	363	27.25334	10903	1.344713	584
163046 E1	1y Convalescent (CAA+)	163046 E1	54.87736	2174	2.406618	362	6.6621687	106	13.12460086	903	1.04754	672	0.056102	275	0.078386	387	1.354365	399	4.978356	2092	1.082265	518
163016 A9	1y Convalescent (CAA+)	163016 A9	37.95773	1405	3.128577	451	5.71560663	102	7.354695262	623	0.315683	343	0.024719	243	0.032282	371	0.063224	180	7.627057	3124	7.721665	2215
153051 F5	1y Convalescent (CAA+)	153051 F5	371.471	23218	2.258915	344	6.8804462	107	4.446939322	482	0.490507	422	0.066899	286	0.212624	433	0.419426	236	10.65089	4310	1.594566	647
153005 F6	1y Convalescent (CAA+)	153005 F6	78.5595	3358	3.497117	497	NaN	83	4.797633136	499	0.273775	324	0.0208	239	NaN	319	0.097558	185	7.235566	2971	2.349035	838
153003 A3	1y Convalescent (CAA+)	153003 A3	84.60594	3677	2.283577	347	11.926112	138	4.942026032	506	0.446173	402	0.006123	224	0.026565	369	0.049115	178	9.360399	3803	3.652909	1170
193051 F4	1y Convalescent (CAA-)	193051 F4	211.5552	11461	2.37385	358	23.7546216	267	6.09697241	562	0.198961	290	0.060028	279	NaN	359	0.265702	211	5.490724	2291	1.19768	547
193006 F2	1y Convalescent (CAA-)	193006 F2	159.4903	8055	2.447535	367	1.42950623	91	2.837326197	404	0.21874	299	0.03256	251	0.148212	411	0.40731	234	11.59598	4682	0.990608	495
183084 E9	1y Convalescent (CAA-)	183084 E9	124.452	5918	1.919921	303	6.6621687	106	3.043745554	414	0.166046	275	0.045308	264	NaN	344	0.034684	176	9.604982	3899	1.00257	498
183031 E5	1y Convalescent (CAA-)	183031 E5	43.73182	1659	2.797584	410	7.09268051	108	3.064386403	415	0.295824	334	0.081629	301	NaN	347	0.157235	194	6.853949	2822	1.261291	563
173025 C2	1y Convalescent (CAA-)	173025 C2	63.61928	2598	1.994662	312	8.44364857	115	13.2687954	910	0.748407	538	0.064936	284	0.003927	361	0.315489	219	14.37289	5778	1.570795	641
173018 B9	1y Convalescent (CAA-)	173018 B9	21.51239	741	3.257085	467	10.8298612	130	9.539563721	729	0.289207	331	0.064936	284	NaN	355	0.290677	215	7.875072	3221	1.138003	532
163096 E2	1y Convalescent (CAA-)	163096 E2	19.08149	652	2.545548	379	11.2521799	133	3.766068674	449	0.501598	427	0.091451	311	0.038013	373	0.616019	269	3.865286	1661	10.42508	2914
153084 A7	1y Convalescent (CAA-)	153084 A7	153.3393	7670	2.700213	398	8.79522084	117	8.467839017	677	1.691171	959	0.0777	297	0.032282	371	NaN	161	5.768433	2399	1.134023	531
153058 A6	1y Convalescent (CAA-)	153058 A6	35.33846	1293	3.552961	504	15.2038107	166	5.251419981	521	0.247342	312	0.063954	283	NaN	336	0.327839	221	6.523253	2693	1.721262	679
153000 A2	1y Convalescent (CAA-)	153000 A2	156.3508	7858	2.291793	348	10.0910399	125	3.188227513	421	0.441742	400	0.039423	258	NaN	329	NaN	161	7.650075	3133	1.165858	539
183082 E6	Acute (CAA+)	183082 E6	536.0377	36825	5.93886	809	12.056833	139	82.57570368	4280	6.626045	3133	0.315772	539	0.192097	426	115.911	27490	15.21211	6110	2.175575	794
173088 D9	Acute (CAA+)	173088 D9	71.56552	2997	10.97133	1478	11.2521799	133	85.5961418	4427	8.307851	3868	0.132728	353	4.910247	1986	61.42151	13964	12.44336	5016	1.443931	609
173017 B6	Acute (CAA+)	173017 B6	235.9756	13140	5.025389	691	13.9986664	155	35.25146874	1978	14.62272	6612	0.245865	468	2.890951	1324	14.84883	3164	31.6235	12653	2.45145	864
173007 B5	Acute (CAA+)	173007 B5	426.0195	27582	4.838265	667	39.5836525	556	142.1609687	7181	15.22119	6871	0.233069	455	2.126817	1072	20.78934	4470	16.69141	6696	3.359022	1095
163116 B3	Acute (CAA+)	163116 B3	68.94377	2864	7.60246	1027	27.1493666	318	170.2053769	8547	15.40381	6950	0.227164	449	2.459976	1182	199.4945	49174	34.8679	13955	2.895906	977
163046 F8	Acute (CAA+)	163046 F8	301.3785	17856	3.24104	465	7.89014168	112	10.8995925	795	1.617001	926	0.084575	304	0.139455	408	20.27654	4356	4.211887	1795	0.950722	485
163016 B1	Acute (CAA+)	163016 B1	76.58126	3255	5.359479	734	17.1998587	186	37.88448436	2106	4.665286	2273	0.060028	279	0.752078	615	28.80855	6278	19.07972	7644	1.899213	724
153051 D8	Acute (CAA+)	153051 D8	1001.278	80904	5.545326	758	17.759231	192	32.57703671	1848	12.36404	5633	0.202562	424	0.898466	664	59.39961	13476	20.70915	8292	2.762283	943
153005 D7	Acute (CAA+)	153005 D7	146.0177	7217	6.26161	851	7.09268051	108	67.43005206	3543	11.38994	5210	0.08654	306	0.573354	555	8.489179	1811	6.610441	2727	1.471696	616
153003 A4	Acute (CAA+)	153003 A4	360.6067	22368	12.69741	1713	32.9962188	420	761.2626919	37373	39.89048	17439	0.42414	649	1.126133	740	240.0643	59976	54.77523	21985	3.977763	1253
193051 F3	Acute(CAA-)	193051 F3	426.6336	27632	3.46518	493	48.6145876	778	42.16260875	2314	3.015559	1546	0.115034	335	4.876583	1975	8.681474	1851	20.30955	8133	1.677725	668
193006 F1	Acute(CAA-)	193006 F1	761.5178	57302	6.123431	833	20.6712281	226	64.92248367	3421	7.197527	3383	0.175015	396	1.459731	851	44.26321	9866	27.59588	11040	2.734761	936
183084 E8	Acute(CAA-)	183084 E8	288.5962	16911	4.493901	623	10.242624	126	27.47418635	1600	2.712503	1412	0.087522	307	0.116138	400	4.924826	1084	33.67744	13477	0.846905	459
183031 E4	Acute(CAA-)	183031 E4	131.4247	6332	4.861682	670	11.1130075	132	27.3507151	1594	2.159449	1167	0.134694	355	1.339384	811	25.49697	5526	12.22781	4931	1.543056	634
173025 C1	Acute(CAA-)	173025 C1	131.7757	6353	3.918488	550	13.9986664	155	55.19922694	2948	25.89306	11466	0.216338	438	2.948686	1343	12.96274	2757	49.54164	19868	3.519722	1136
173018 B8	Acute(CAA-)	173018 B8	28.69724	1019	8.462216	1141	12.4415872	142	192.5379703	9635	2.689902	1402	0.156327	377	1.872874	988	41.45194	9205	11.56551	4670	1.554945	637
163096 F7	Acute(CAA-)	163096 F7	37.02789	1365	6.253939	850	47.788271	756	238.404061	11870	49.12219	21351	0.197642	419	7.341453	2778	110.2109	26047	23.18923	9280	4.567844	1404
153084 A8	Acute(CAA-)	153084 A8	556.4528	38599	8.251624	1113	19.6876955	214	66.97787706	3521	9.897756	4561	0.179933	401	0.084181	389	47.96396	10741	17.47554	7007	1.527202	630
153058 A5	Acute(CAA-)	153058 A5	409.7734	26266	9.755808	1314	38.6325159	535	46.17281075	2509	26.26397	11625	0.094399	314	0.318562	469	112.6864	26673	13.77328	5541	2.840895	963
153000 A1	Acute(CAA-)	153000 A1	416.1632	26782	3.8313	539	71.5444629	1521	14.25750108	958	2.21807	1193	0.540451	767	0.862584	652	9.170377	1953	67.8311	27281	2.541999	887
37-CHM-001 D6	MIS-C	37-CHM-001 D6	364.6812	22686	10.57956	1425	60.3324853	1126	206.0426038	10293	62.88552	27148	0.313803	537	1.372466	822	75.98034	17512	102.1601	41285	10.05057	2817
204026 D5	MIS-C	204026 D5	20.04665	687	3.783685	533	8.26284603	114	112.507169	5737	0.630429	485	0.120932	341	0.055269	379	1.596296	443	26.88821	10757	1.110139	525
203064 D4	MIS-C	203064 D4	101.5641	4603	8.20645	1107	59.6530791	1104	284.0741884	14096	91.97109	39275	0.206498	428	2.657136	1247	50.60239	11368	58.37203	23442	4.642015	1423
203063 D3	MIS-C	203063 D3	1011.437	81940	10.63136	1432	44.5884154	674	524.6505369	25828	37.32219	16347	0.359111	583	1.198162	764	64.96015	14821	41.89966	16784	5.51139	1646
203060 D2	MIS-C	203060 D2	257.8869	6184	13.9142	942	83.6251539	607	1447.567664	35544	500.7464	102925	0.935007	693	2.162291	725	297.7785	35938	110.2371	22124	12.03461	1776
203055 D1	MIS-C	203055 D1	67.09489	2771	7.413051	1002	38.2646163	527	1776.509182	86941	11.51193	5263	0.152393	373	1.168142	754	19.91609	4276	16.31298	6546	2.620701	907
203049 C9	MIS-C	203049 C9	71.07466	2972	11.91362	1606	21.459851	236	1847.397085	90403	0.481637	418	1.793404	2036	0.113227	399	64.97663	14825	30.2163	12089	2.463264	867
203046 C7, C8	MIS-C	203046 C7, C8	71.58513	2998	3.648553	516	13.884472	154	8.570897242	682	0.401886	382	0.104224	324	0.29792	462	10.46475	2225	10.45508	4233	1.642093	659
203041 C5, C6	MIS-C	203041 C5, C6	404.8144	25867	5.033176	692	33.2589857	425	53.32832424	2857	4.904206	2378	0.153377	374	0.274353	454	20.0423	4304	15.90662	6385	2.734761	936
203040 C3, C4	MIS-C	203040 C3, C4	210.3145	11377	14.50176	1961	59.0293781	1084	3791.399258	185356	270.5069	110759	0.397535	622	6.926112	2643	77.39216	17859	80.06504	32260	6.130082	1805
09092020NHD-21	Healthy Adult	09092020NHD-21	1.894622	137	0.758415	167	NaN	89	NaN	250	0.037486	216	0.015905	234	NaN	343	0.056203	179	1.012209	569	NaN	239
09092020NHD-21	Healthy Adult	09092020NHD-21	13.30884	453	0.873026	180	NaN	79	2.17663623	372	0.033173	214	0.0777	297	0.066814	383	NaN	166	1.469193	742	0.368996	340
09092020NHD-20	Healthy Adult	09092020NHD-20	5.356065	217	1.064729	202	NaN	89	2.238586552	375	0.089545	240	0.024719	243	NaN	350	0.137575	191	1.303118	679	0.165905	290
09092020NHD-18	Healthy Adult	09092020NHD-18	10.41427	361	0.829074	175	4.60089399	98	0.68883925	300	0.052618	223	0.14846	369	0.066814	383	NaN	163	1.022811	573	0.296126	322
09092020NHD-17	Healthy Adult	09092020NHD-17	4.073091	185	1.073384	203	NaN	84	1.866846576	357	0.037486	216	0.039423	258	NaN	358	0.150704	193	0.773091	479	0.063146	265
09092020NHD-17	Healthy Adult	09092020NHD-17	4.156145	187	0.951766	189	2.15015749	92	0.274948861	280	0.041804	218	0.01199	230	NaN	345	NaN	169	0.682434	445	NaN	227
09092020NHD-16	Healthy Adult	09092020NHD-16	7.712331	281	0.899325	183	NaN	84	1.164369184	323	0.00747	202	0.02276	241	NaN	351	0.041947	177	2.308243	1062	0.075557	268
09092020NHD-15	Healthy Adult	09092020NHD-15	2.946414	159	1.021384	197	6.6621687	106	1.22637205	326	0.043965	219	0.023739	242	0.040883	374	0.163746	195	1.078442	594	0.08794	271
09092020NHD-13	Healthy Adult	09092020NHD-13	3.434851	170	0.322404	119	NaN	76	1.040349499	317	0.035329	215	0.036481	255	0.038013	373	0.104303	186	1.157826	624	0.141354	284
09092020NHD-12	Healthy Adult	09092020NHD-12	6.672139	252	0.908079	184	2.15015749	92	0.895633789	310	0.054784	224	0.005147	223	NaN	349	NaN	164	1.456025	737	NaN	239
09092020NHD-47	Healthy Adult	09092020NHD-47	30.30641	1084	2.406618	362	4.60089399	98	0.895633789	310	0.466118	411	0.03354	252	0.092883	392	1.415136	410	1.97341	934	0.602595	398
COVID-09092020-	Acute COVID19	COVID-09092020-	26.81046	944	3.870947	544	14.1120312	156	35.49832507	1990	0.93133	620	0.016884	235	0.250813	446	31.87821	6981	7.806051	3194	1.201657	548
COVID-09092020-	Acute COVID19	COVID-09092020-	9.658498	338	1.869984	297	NaN	82	49.66849538	2679	0.786293	555	0.02178	240	0.200891	429	1.001909	336	5.961147	2474	0.538305	382
COVID-09092020-	Acute COVID19	COVID-09092020-	9.988935	348	1.919921	303	3.94072339	96	1.866846576	357	0.557089	452	0.131745	352	1.480806	858	9.509516	2024	1.041361	580	0.874872	466
COVID-09092020-	Acute COVID19	COVID-09092020-	7.747521	282	2.918974	425	3.16161906	94	0.005380432	267	0.166046	275	0.03256	251	NaN	337	0.011992	173	0.998953	564	0.296126	322
COVID-09092020-	Acute COVID19	COVID-09092020-	24.96574	872	4.736701	654	8.07842239	113	49.97692171	2694	1.94091	1070	0.615391	843	0.976274	690	4.969948	1093	2.161868	1006	0.746915	434
COVID-09092020-	Acute COVID19	COVID-09092020-	14.30607	486	3.385247	483	10.3922218	127	17.98494465	1139	0.949199	628	0.045308	264	0.09869	394	11.55913	2457	2.350034	1078	0.758923	437
COVID-09092020-	Acute COVID19	COVID-09092020-	12.81826	437	1.399071	241	5.18520532	100	3.47716469	435	0.512691	432	0.050214	269	0.168673	418	9.961862	2119	3.375471	1472	0.578498	392
COVID-08202020-	Acute COVID19	COVID-08202020-	18.69184	638	1.585193	263	NaN	83	1.722254399	350	0.393035	378	0.043346	262	0.078386	387	5.040077	1107	0.473585	367	0.38112	343
COVID-08202020-	Acute COVID19	COVID-08202020-	19.49666	667	5.227572	717	7.69774095	111	11.16744841	808	1.648463	940	0.070826	290	0.151133	412	9.026793	1923	16.49464	6618	0.922787	478
COVID-08202020-	Acute COVID19	COVID-08202020-	28.6723	1018	2.675834	395	8.26284603	114	12.65080329	880	0.79744	560	0.073772	293	0.130704	405	3.203718	746	1.70062	830	0.654761	411
COVID-08202020-	Acute COVID19	COVID-08202020-	11.12392	383	1.416058	243	5.45619182	101	2.837326197	404	0.192373	287	0.026679	245	0.035146	372	0.916687	321	3.066432	1353	0.255539	312
COVID-08202020-	Acute COVID19	COVID-08202020-	1.792071	135	3.361242	480	4.90086951	99	13.39238901	916	0.120085	254	0.071808	291	0.174525	420	9.251665	1970	2.715166	1218	0.80693	449
COVID-08202020-	Acute COVID19	COVID-08202020-	54.79322	2170	1.811608	290	9.13461371	119	34.63431754	1948	0.888907	601	0.097346	317	0.436825	509	3.61123	825	3.904111	1676	1.293079	571
COVID-08202020-	Acute COVID19	COVID-08202020-	17.96247	612	2.135325	329	12.8159518	145	3.559711953	439	1.085564	689	0.21929	441	0.552547	548	6.521751	1406	2.821927	1259	1.078282	517
COVID-08202020-	Acute COVID19	COVID-08202020-	7.035342	262	2.357454	356	6.43727739	105	0.68883925	300	0.384185	374	0.108155	328	0.08708	390	2.20053	555	0.983043	558	0.437633	357
COVID-05282020-	Acute COVID19	COVID-05282020-	40.4392	1513	2.085754	323	10.0910399	125	4.673863029	493	0.32893	349	0.168129	389	0.283188	457	7.337829	1573	3.211928	1409	1.217563	552
COVID-05282020-	Acute COVID19	COVID-05282020-	49.1602	1906	3.297172	472	10.0910399	125	0.647470757	298	0.980478	642	0.104224	324	0.183308	423	12.55694	2670	1.981269	937	0.902827	473
COVID-05282020-	Acute COVID19	COVID-05282020-	44.28902	1684	6.092696	829	17.0097422	184	69.64976129	3651	1.556345	899	0.111103	331	0.48129	524	58.63175	13291	20.91769	8375	0.994596	496
COVID-05282020-	Acute COVID19	COVID-05282020-	32.03889	1155	2.951285	429	9.13461371	119	9.189211411	712	0.426237	393	0.094399	314	NaN	358	2.248487	564	3.398823	1481	0.870878	465
COVID-05282020-	Acute COVID19	COVID-05282020-	91.31458	4038	1.944857	306	16.1294648	175	4.694491691	494	0.508253	430	0.05512	274	0.407214	499	38.21436	8448	3.102817	1367	1.118101	527
COVID-05282020-	Acute COVID19	COVID-05282020-	12.72574	434	1.944857	306	NaN	74	4.446939322	482	0.410739	386	0.048252	267	0.29792	462	3.477519	799	5.773574	2401	0.3892	345
COVID-05282020-	Acute COVID19	COVID-05282020-	48.79179	1889	1.509243	254	8.07842239	113	2.424423556	384	0.229736	304	0.036481	255	0.107409	397	0.077095	182	3.948105	1693	0.522216	378
COVID-05282020-	Acute COVID19	COVID-05282020-	26.14827	918	2.291793	348	2.15015749	92	55.98045735	2986	0.819739	570	0.058065	277	0.168673	418	3.302071	765	7.765145	3178	0.477937	367
COVID-05282020-	Acute COVID19	COVID-05282020-	19.90952	682	1.416058	243	8.96635802	118	1.123031419	321	0.37755	371	0.048252	267	0.280243	456	1.287831	387	2.023172	953	0.65075	410
COVID-05282020-	Acute COVID19	COVID-05282020-	15.84173	538	1.593617	264	4.28223997	97	9.27164888	716	0.601526	472	0.054139	273	0.156977	414	2.608438	632	5.035044	2114	0.288015	320
COVID-05282020-	Acute COVID19	COVID-05282020-	64.20531	2627	1.211237	219	3.57029677	95	2.445070868	385	0.12664	257	0.152393	373	0.026565	369	5.801879	1260	4.036066	1727	0.449729	360
COVID-05282020-	Acute COVID19	COVID-05282020-	6.963102	260	0.696218	160	NaN	85	4.054942028	463	0.083015	237	0.037462	256	NaN	357	0.234228	206	0.583532	408	0.034038	258
S008	Standards	S008	NaN	92	NaN	84	2.59260266	100	NaN	257	NaN	198	0.001109	220	0.011856	368	NaN	164	0.007549	199	NaN	249
S007	Standards	S007	0.682277	127	0.221558	132	NaN	79	0.437478795	309	0.090699	282	0.143115	509	0.310475	571	0.179281	226	0.130157	288	0.129801	313
S006	Standards	S006	1.782421	173	1.137679	346	2.30044699	98	1.604433523	422	0.339687	507	0.586493	1408	1.263342	1204	0.768046	432	0.613274	650	0.283222	389
S005	Standards	S005	7.2427	492	4.302457	1160	4.31052133	116	5.82066289	831	1.358512	1414	2.466558	5209	5.524812	3979	2.841455	1236	2.431184	2047	1.540241	1024
S004	Standards	S004	19.07149	1413	12.62174	3475	16.8118824	432	24.33047556	2630	5.989665	5466	10.04687	20490	22.48564	14785	10.85454	4675	10.14472	8125	6.024228	3335
S003	Standards	S003	75.06727	7471	53.78816	16027	64.5882462	4469	87.35046206	8766	21.14764	18460	35.78254	72225	82.77428	52116	37.05896	17055	35.83279	28840	22.08092	11762
S002	Standards	S002	344.1422	50449	223.0646	72923	269.95242	62894	377.1376287	37032	90.60593	75592	154.8871	310816	331.6874	197233	173.4336	89036	150.4121	123495	89.69013	47913
S001	Standards	S001	1512.414	326006	1185.338	433503	1056.78449	508391	1547.497484	151340	355.2642	269917	610.9909	1219541	1373.165	704294	780.1561	448151	631.4399	530359	374.8746	203207